Auger recombination mechanisms in semiconductor nanoheterostructures. Part 1. Quantum wells (Review)

© G.G. Zegrya, N.L. Bazhenov

Ioffe Institute,
194021 St. Petersburg, Russia

E-mail: zegrya@theory.ioffe.ru

Received November 10, 2025
Revised November 18, 2025
Accepted November 18, 2025

This review is devoted to the mechanisms of Auger recombination in semiconductor nanoheterostructures. A distinctive feature of nanoheterostructures is the strong spatial heterogeneity attributable to the existence of heteroboundary. Heteroboundaries have a fundamental effect on the amount of energy and on the behavior of charge carrier wave functions in quantum-dimensional heterostructures and, as shown in this review, significantly affect the macroscopic properties of semiconductor nanostructures. The presence of a heterogeneous boundary affects the electron-electron (hole-hole) interaction in quantum structures, and this effect is fundamental. The heteroboundary removes the restrictions imposed on interelectronic collision processes by the laws of conservation of energy and momentum, which leads to the appearance of thresholdless, temperature-weakly dependent Auger recombination channels. This review studies the main mechanisms of Auger recombination of nonequilibrium charge carriers in semiconductor heterostructures with quantum wells (Part 1), quantum filaments, and quantum dots (Part 2). It is shown that there are three fundamentally different Auger recombination mechanisms: thresholdless, quasi-threshold, and threshold. The rate of the thresholdless process is weakly dependent on temperature. The threshold energy of the quasi-threshold process significantly depends on the width of the quantum well and is close to zero for narrow quantum wells. It is shown that thresholdless and quasi-threshold Auger processes prevail in narrow quantum wells, while thresholdless and quasi-threshold Auger processes prevail in wide quantum wells. A critical width of the quantum well has been found at which the quasi-threshold Auger recombination channel transforms into a three-dimensional threshold Auger process. The influence of phonons on Auger recombination processes in quantum wells is also analyzed. It is shown that for narrow quantum wells, the Auger process involving phonons becomes resonant, which leads to an increase in the Auger recombination coefficient involving phonons. The effect of relaxation processes on Auger recombination mechanisms in homogeneous semiconductors is considered separately. It is shown that taking into account relaxation processes leads to the removal of the energy threshold for Auger recombination processes.

Keywords: semiconductor heterostructures, quantum wells, quantum filaments, quantum dots, heterogeneity, Auger recombination, microscopic theory.

DOI: 10.61011/SC.2025.09.62833.8766

1. Introduction

The processes of recombination of nonequilibrium carriers in semiconductors can be of two types: 1) processes of radiative recombination and 2) processes of nonradiative recombination. If photon emission occurs during interband recombination of an electron-hole pair, then radiative recombination takes place, otherwise electron-hole recombination is nonradiative. There is a large number of different mechanisms of nonradiative recombination in semiconductors [1]: recombination through impurities and defects in the crystal lattice, multiphonon emission, surface recombination, Auger recombination, etc. At high levels of excitation of nonequilibrium charge carriers, the main process of nonradiative recombination in semiconductors is the Auger process [1,2]. In the case of Auger recombination (AR), the energy of the recombining electron-hole pair is transferred to a third carrier (electron or hole), which, absorbing the energy transferred to it, transits into a highly excited state. In semiconductors, this phenomenon was called the Auger process by analogy with the well-known Auger effect in atoms, discovered by Pierre Auger in 1925 [3].

Auger recombination processes in semiconductors are usually classified according to which energy zones the initial and final states of the particles involved in the recombination process belong to. The following Auger recombination processes are distinguished in homogeneous semiconductors [1,4]: CHCC, CLCC, CHHS, CHHL, etc.. The letters C, H, L, and S denote the states of electrons in the conduction band, heavy and light holes in the valence band, and holes in the spin-split band, respectively. For example, in the CHCC process (Figure 1, *a*), as a result of the Coulomb interaction of two electrons, one of them recombines with a heavy hole, and the other absorbs the energy transferred to it and transits into a highly excited state in the conduction band. In the CHHS process

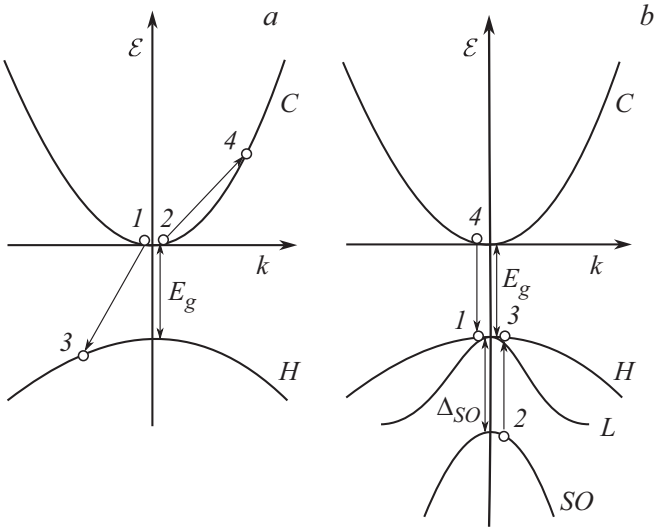

Figure 1. Scheme of electron and hole transitions during Auger recombination: *a* — transitions with energy transfer to an electron (CHCC processes), *b* — transitions with energy transfer to a hole during its transition to a spin-orbitally split zone (CHCC process). Here Δ_{SO} is the energy of the spin-orbit coupling; „1“ and „2“ are the initial states of the particles; „3“ and „4“ are the final states.

(Figure 1, *b*), a heavy hole recombines with an electron, and the second heavy hole transits into the spin-split zone as a result of the Coulomb interaction.

The Auger recombination process is threshold in most cases in homogeneous semiconductors, and the Auger recombination rate G varies exponentially with temperature [1]. It should be emphasized that this statement is valid for the case when the AR process is considered in the framework of the first-order theory of perturbation by electron-electron (hole-hole) interaction. At high excitation levels, due to electron-electron (hole-hole) scattering processes, AR becomes a thresholdless process, since relaxation processes remove the restrictions imposed by the laws of conservation of energy and momentum at AR. In a bulk semiconductor, relaxation processes play the same role as heteroboundary in semiconductor heterostructures [5][1] (see *Appendix* I). The effect of relaxation processes on the Auger recombination mechanism was first considered in Ref. [5]. It is shown in this paper that the effects of charge carrier relaxation on carriers change not only the value of the Auger recombination coefficient, but also its dependence on temperature.

In addition, the thresholdless case is represented by the processes of Auger recombination with the transition of a hole into a spin-split band in semiconductors, where the magnitude of the spin-orbit splitting Δ_{so} is close to the band gap E_g. This takes place in InAs and GaSb semiconductors and CdHgTe-based heterostructures. In this case, the Auger process has a „resonant“ character, and the recombination rate does not have an exponential dependence on temperature.

It should be noted that in lead chalcogenides (PbS, PbSe, and PbTe) with a linear dispersion law, Auger recombination is suppressed due to failure to comply with the law of conservation of energy and momentum in such a process.

Let us briefly consider the nature of the formation of the Auger recombination threshold in homogeneous semiconductors using the example of the CHCC process (Figure 1, *a*). In the case of such a recombination process, two fundamental conservation laws of quasi-momentum and energy must be fulfilled:

$$\mathbf{k}_1 + \mathbf{k}_2 = \mathbf{k}_3 + \mathbf{k}_4, \tag{1}$$

$$E_1 + E_2 = E_3 + E_4. \tag{2}$$

Here $\mathbf{k}_1$, $\mathbf{k}_2$ and E_1, E_2 are quasi-momenta and energies of particles in the initial states „1“ and „2“; $\mathbf{k}_3$, $\mathbf{k}_4$ and E_3, E_4 are quasi-momenta and energies in the final states „3“ and „4“. A quasi-momentum is in many ways similar to the ordinary momentum of a particle. At the same time, there is a significant difference between them because the quasi-momentum is a value determined only with accuracy to the constant vector of the inverse lattice $\hbar\mathbf{b}$. The momentum values $\mathbf{p} = \hbar\mathbf{k}$, which differ by this amount $\hbar\mathbf{b}$, are physically equivalent [6]. The requirement of simultaneous implementation of conservation laws (1) and (2) means that the total kinetic energy of the electrons „1“ and „2“ and the hole „4“ in the initial state must exceed a certain threshold value E_{th} [1]. Consequently, in a homogeneous straight-band semiconductor, in the framework of the 1st order of perturbation theory for electron-electron coupling, the Auger recombination process is threshold, and its rate contains an exponential dependence on temperature $G \propto \exp(-E_{\text{th}}/T)$, where $E_{\text{th}} = 2m_e/m_h E_g$, m_e is the effective mass of an electron, m_h is the effective mass of a heavy hole, T is a temperature in energy units. An algorithm for calculating the threshold energy for the Auger recombination process is given in [1], that takes into account the nonparabolic dispersion law for an excited electron. It is interesting to note that the „2“ multiplier in the expression for E_{th} appears due to the „Dirac“ energy spectrum for an excited electron, i. e., the nonparabolicity of the dispersion law. This will be described in detail in the next paragraph.

In the first works on Auger recombination in homogeneous semiconductors, the overlap integrals between the states of electrons and holes were considered as constants, the values of which were estimated from various simplified models ([7], etc.). The correct calculation of overlap integrals for Auger processes based on the Kane model was performed for the first time in Refs. [8–10]. The correct expression for the Auger recombination rate of the CHCC process was obtained for the first time in Ref. [10] in the

[1] *Appendices* I, II, and III are presented in the 2nd part of the article.

framework of the Kane model:

$$G_{3D} = 6\sqrt{2\pi^5}\,\frac{m_e e^4 \hbar^3}{\kappa_0}\,(E_g^{5/2} T^{1/2} m_e^{1/2} m_h^{3/2})^{-1} \times \exp\left(-\frac{2m_e}{m_h}\frac{E_g}{T}\right), \quad (3)$$

where κ_0 is the static dielectric constant.

It is shown in this paper that the overlap integrals are zero within the framework of the simplest two-band model, as discussed in Ref. [7]. Thus, it is necessary to use the Kane multi-zone model to calculate the Auger recombination rate. The Kane model for homogeneous semiconductors is described in many textbooks [1].

This review is devoted to the mechanisms of Auger recombination in semiconductor nanoheterostructures. A distinctive feature of nanoheterostructures, as already noted above, is the strong spatial heterogeneity caused by the existence of heterogeneous boundaries. Heteroboundaries have a fundamental effect on the amount of energy and on the behavior of the wave functions of charge carriers in quantum-dimensional heterostructures. The heteroboundary removes the restrictions imposed on interelectronic collision processes by the laws of conservation of energy and momentum, which leads to the appearance of thresholdless, temperature-weakly dependent Auger recombination channels.

The monograph of reputable experts in the field of physics of AR processes [1] notes that calculating the probability of AR in homogeneous semiconductors is a difficult task. This is primarily due to the need to calculate the overlap integrals of the Bloch amplitudes related to different bands. As it turned out, calculating the probability of AR in semiconductor nanostructures is an even more difficult task. As noted above, the heterostructures are spatially heterogeneous. We have a qualitatively different semiconductor environment. In nanostructures, the spectrum and wave functions of charge carriers change qualitatively and quantitatively, and the problem of boundary conditions for wave functions arises. In this review, we wanted to draw attention to fundamental aspects concerning the mechanisms of AR in nanoheterostructures. We present a detailed microscopic analysis of the AR mechanisms in quantum wells, quantum filaments, and quantum dots. The details of calculating the spectra, wave functions, and matrix elements of the Coulomb interaction between particles are described, taking into account the spatial symmetry of the problem. This style of presentation of the material makes the review useful for experimentalists, young, novice scientists and specialists working in the field of physics of semiconductor nanostructures. We do not pretend to provide a full review of publications on this topic. At the end of the list of references, we cite several publications on AR that use the ideology of this review to solve specific problems.

2. The influence of spatial heterogeneity of the heterogeneous boundary on the mechanisms of Auger recombination. New Auger recombination mechanism in semiconductor heterostructures

Currently, the main objects of research in semiconductor physics are heterostructures such as single heterobarriers, quantum wells, quantum filaments, quantum dots, superlattices, etc. A distinctive feature of such structures, as already noted above, is the strong spatial heterogeneity caused by the existence of heteroboudaries. Previously, it was believed that the efficiency of nonradiative Auger processes in heterostructures corresponds to the usual bulk Auger processes [11,12]. As will be shown below, the presence of heterogeneous boundaries qualitatively and quantitatively affects the processes of electron-electron (hole-hole) interaction in semiconductor quantum structures.

This section describes a new mechanism of Auger recombination of the bulk states, the so-called thresholdless Auger process. The rate of such a thresholdless process has a power-law dependence on temperature, and the process itself is the dominant mechanism of nonradiative recombination of nonequilibrium charge carriers in heterostructures and in nanometer-sized structures (see sec. 3, 4, 5). Let's give a qualitative interpretation of the new Auger recombination mechanism [13].

1. Auger recombination processes constraints related to the law of conservation of momentum are lifted if at least one of the quasi-particles (an electron, for certainty) is located near a heterogeneous boundary or in the region of sub-barrier motion. The wave function of the quasi-particles in this region is a wave packet with different quasi-momentum values, among which there are momenta corresponding to the final momentum of the excited Auger electron.

2. The transfer of energy from a recombining electron-hole pair to a fast Auger electron has a resonant character. The electron receives the momentum necessary for the transition to the final highly excited state from interaction with the heterogeneous boundary, but not from interaction with another electron. At the same time, there is no law of conservation of momentum in the matrix element for the component perpendicular to the heterogeneous boundary, and, as a result, the Auger transition rate does not have the usual exponential temperature dependence for a homogeneous semiconductor. (see formula (3)).

3. The emission of fast Auger electrons occurs mainly in the direction of the axis perpendicular to the heterogeneous boundary, i.e. axes of maximum spatial heterogeneity in the system. The electrons are ejected over the barrier in a direction perpendicular to the heterogeneous boundary, in a narrow range of angles $\Delta\vartheta \sim (T/E_g)^{1/2} \ll 1$.

Here we consider the case when the height of the heterobarrier for an electron V_c (or a hole V_v) is less than

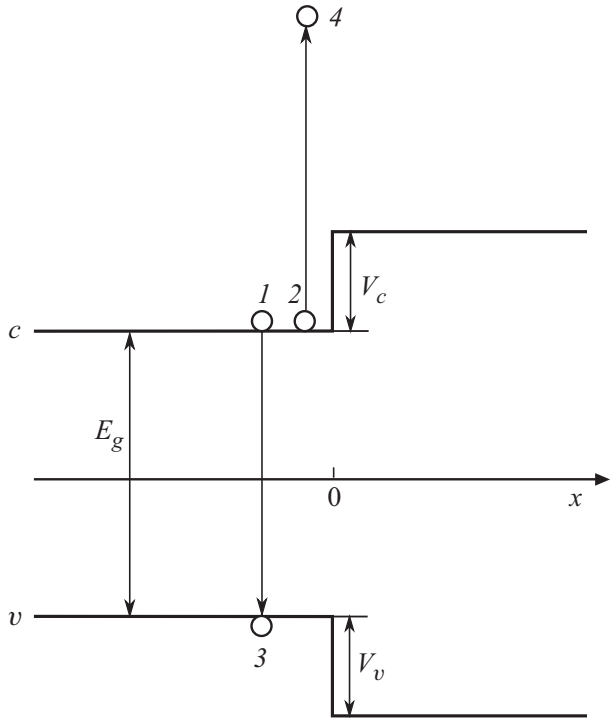

Figure 2. Schematic representation of the band diagram of the heterojunction. Here, the point $x = 0$ corresponds to a heterogeneous boundary, and „1“ and „2“ are the initial states for electrons; „3“ and „4“ are the final states.

the band gap width of a narrow-band semiconductor (see Figure 2).

A detailed analysis of threshold and thresholdless Auger recombination mechanisms for a single heterobarrier was performed in [13] (Figure 2). The conditions under which the thresholdless channel prevails over the threshold channel are analyzed. For quantum wells, such a detailed analysis of the Auger recombination mechanisms is given in sec. 3. The possibility of removing the threshold for the Auger recombination process in quantum wells during the transition of excited carriers to the continuous part of the spectrum is analyzed in Ref. [14]. However, this paper lacks a microscopic theory of the thresholdless process and there is no theoretical analysis of the competition between threshold, quasi-threshold, and thresholdless Auger recombination mechanisms at different temperatures and at different quantum well widths. Only the thresholdless Auger recombination channel is considered in Refs. [15,16], which corresponds to small transmitted momenta in the Coulomb interaction of particles (for the CHCC process), neglecting the spin-orbital interaction. A rigorous theory for the thresholdless Auger recombination channel for the case of quantum wells, quantum filaments, and quantum dots will be given in sec. 3, 4 and 5. The first direct experiment to observe the thresholdless Auger recombination channel at $T = 77\,\mathrm{K}$ was performed in Ref. [17].

3. Auger recombination mechanism in semiconductor quantum wells. thresholdless and quasi-threshold Auger recombination channels

The purpose of this section is to theoretically study the main mechanisms of Auger recombination of nonequilibrium carriers in semiconductor quantum wells. It will be shown that there are three fundamentally different Auger recombination mechanisms in quantum wells: (i) a threshold mechanism similar to the Auger process in a homogeneous semiconductor, (ii) a quasi-threshold mechanism whose threshold energy significantly depends on the width of the quantum well, (iii) a thresholdless mechanism not present in a homogeneous semiconductor. For the threshold Auger recombination process in a quantum well, the threshold energy is close to the threshold energy of a homogeneous semiconductor. Conversely, due to the low threshold energy, the rate of the quasi-threshold process in sufficiently narrow quantum wells is weakly dependent on temperature. For this reason, in rather narrow quantum wells there is no clear separation between thresholdless and quasi-threshold Auger recombination mechanisms and they merge into one thresholdless Auger process. As the width of the quantum well increases, the threshold energy of the quasi-threshold process increases and tends to a bulk value. The thresholdless AR channel behaves completely differently. As the width of the quantum well increases, its rate decreases sharply, tends to zero, and this mechanism disappears during the transition to a homogeneous semiconductor. In this section, we will obtain conditions under which the thresholdless Auger recombination mechanism prevails over the threshold one. A critical value of the quantum well thickness will also be found, at which the quasi-threshold and threshold Auger recombination mechanisms merge into one three-dimensional Auger process.

3.1. Basic equations

It is necessary to have the wave functions of charge carriers to analyze the mechanisms of Auger recombination and find the rate of the Auger process. As has already been established for bulk Auger processes, the wave functions of the carriers must be calculated in the multi-band approximation [10]. We will use the four-band Kane model, which most accurately describes the wave functions and carrier spectrum in narrow-band semiconductors $A^{III}B^{V}$ [18].

3.1.1. Wave functions in a homogeneous semiconductor

For most semiconductors $A^{III}B^{V}$, the wave functions of the conduction zone in the center of the Brillouin band are described by the representation Γ_6^+, and the wave functions of the valence band are described by the representations Γ_7^+ and Γ_8^+. The first two of them are doubly degenerate, and the last one is fourfold degenerate. The corresponding

equations for wave functions can be written in differential form. Usually, the basis wave functions of the conduction band and the valence band are taken as eigenfunctions of the angular momentum [18,19]. However, a different representation of the basic functions is more suitable for our purposes:

$$|s\uparrow\rangle,\ \ |s\downarrow\rangle,\ \ |x\uparrow\rangle,\ \ |x\downarrow\rangle,\ \ |y\uparrow\rangle,\ \ |y\downarrow\rangle,\ \ |z\uparrow\rangle,\ \ |z\downarrow\rangle, \tag{4}$$

where $|s\rangle$ and $|x\rangle$, $|y\rangle$, $|z\rangle$ are Bloch functions of s- and **p**-type with angular momentum 0 and 1, respectively. The former describe the state of the conduction band, and the latter describe the state of the valence band at the Γ-point. The arrows indicate the direction of the spin. The wave function of charge carriers ψ can be represented as

$$\psi = \Psi_s|s\rangle + \boldsymbol{\Psi}|\mathbf{p}\rangle,$$

where Ψ_s and $\boldsymbol{\Psi}$ are spinors. In the vicinity of the Γ-point, the equations for the envelopes Ψ_s and $\boldsymbol{\Psi}$ have the following form in the spherical approximation:

$$\begin{cases} (E_c - E)\Psi_s - i\hbar\gamma\nabla\boldsymbol{\Psi} = 0, \\ (E_v - \delta - E)\boldsymbol{\Psi} - i\hbar\gamma\nabla\Psi_s + \dfrac{\hbar^2}{2m}(\tilde{\gamma}_1 + 4\tilde{\gamma}_2)\nabla(\nabla\boldsymbol{\Psi}) \\ -\dfrac{\hbar^2}{2m}(\tilde{\gamma}_1 - 2\tilde{\gamma}_2)\nabla\times[\nabla\times\boldsymbol{\Psi}] + i\delta[\boldsymbol{\sigma}\times\boldsymbol{\Psi}] = 0. \end{cases} \tag{5}$$

Here γ is Kane's matrix element [19] having dimension of velocity $\widetilde{\gamma}_1$ and $\widetilde{\gamma}_2 = \widetilde{\gamma}_3$ is the generalized Luttinger parameters [19], $\delta = \Delta_{\mathrm{SO}}/3$, E_c and E_v are the energies of the lower edge of the conduction band and the upper edge of the valence band, m is the mass of the free electron, $\boldsymbol{\sigma} = (\sigma_x, \sigma_y, \sigma_z)$ are the Pauli matrices. If instead of the Luttinger parameters, we phenomenologically introduce the mass of heavy holes describing the interaction with higher zones, then the equations (5) are replaced by the equations obtained in Ref. [20]. It is possible to verify that the equations (5) do not differ from the equations commonly used in the literature [19,21–23]. We neglect the heavy mass term in the first equation of the system (5) for electrons.

Hole states

The expression for Ψ_s can be found from the first equation of the system (5). Substituting Ψ_s into the second equation gives

$$-E\boldsymbol{\Psi} + \frac{\hbar^2}{2m_l}\nabla(\nabla\boldsymbol{\Psi}) - \frac{\hbar^2}{2m_h}\nabla\times[\nabla\times\boldsymbol{\Psi}] + i\delta[\boldsymbol{\sigma}\times\boldsymbol{\Psi}] = 0, \tag{6}$$

where

$$m_l^{-1} = \frac{2\gamma^2}{E_g + \delta - E} + m^{-1}(\widetilde{\gamma}_1 + 4\widetilde{\gamma}_2),$$

$$m_h^{-1} = m^{-1}(\widetilde{\gamma}_1 - 2\widetilde{\gamma}_2).$$

Here m_h coincides with the mass of heavy holes, and m_l coincides with the mass of light holes in the case when the spin-orbit interaction constant is zero; $E_g = E_c - E_v$ is the band gap of the semiconductor. For convenience, it is assumed that $E_v = \delta$. This choice is associated with an increase in the energies of the heavy hole and the light hole at the point Γ by δ and a decrease in the energy of the hole in the spin-orbit (SO) split-off band by 2δ under the influence of spin-orbit interaction (see equation (10)). Equation (6) can be simplified by introducing new functions:

$$\phi = \operatorname{div}\boldsymbol{\Psi} \ \text{ and } \ \eta = \boldsymbol{\sigma}\operatorname{rot}\boldsymbol{\Psi}. \tag{7}$$

After taking the divergence and rotor from equation (6) multiplied by $\boldsymbol{\sigma}$, it turns into a system of two differential equations

$$\begin{cases} -E\phi + \dfrac{\hbar^2}{2m_l}\Delta\phi + i\delta\eta = 0\ , \\ -(E+\delta)\eta + \dfrac{\hbar^2}{2m_h}\Delta\eta - 2i\delta\phi = 0. \end{cases} \tag{8}$$

The Fourier transform of these equations gives a spectrum of light and SO holes for a homogeneous semiconductor

$$\begin{bmatrix} E + \frac{\hbar^2}{2m_l}k^2 & i\delta \\ -2i\delta & E + \frac{\hbar^2}{2m_h}k^2 + \delta \end{bmatrix}\begin{pmatrix}\phi\\ \eta\end{pmatrix} = 0. \tag{9}$$

The characteristic equation has two roots

$$E_{1,2} = -\frac{\delta}{2} - \frac{\hbar^2k^2}{4} \times (m_l^{-1} + m_h^{-1}) \pm \sqrt{2\delta^2 + \left(\frac{\delta}{2} - \frac{\hbar^2k^2}{4}(m_l^{-1} - m_h^{-1})\right)^2}. \tag{10}$$

It should be noted that m_l depends on the energy (see equation (6)). We have the roots $E_1 = \delta$ and $E_2 = -2\delta$ at the point Γ ($k = 0$). The positive solution corresponds to light holes, and the solution with a negative sign corresponds to SO holes.

In the vicinity of the point Γ, the energies $E_{1,2}$ can be expanded into a series in terms of a wave vector in order to relate the effective masses of the light and SO holes m_l, m_{so} with the Luttinger parameters:

$$E_1 \approx \delta - \frac{\hbar^2k^2}{2m_l}, \ \ E_2 \approx -2\delta - \frac{\hbar^2k^2}{2m_{\mathrm{so}}}, \tag{11}$$

where

$$m_l^{-1} = \frac{4\gamma^2}{3E_g} + \frac{(\tilde{\gamma}_1 + 2\tilde{\gamma}_2)}{m}, \ \ m_{\mathrm{so}}^{-1} = \frac{2\gamma^2}{3(E_g + 3\delta)} + \frac{\tilde{\gamma}_1}{m}.$$

An approximate spectrum of light holes can be obtained using the widely used Hamiltonian 4×4 [19]. However, the range of applicability is quite narrow, since usually

$m_l \sim 0.1\, m_h$ and the expansion (11) is valid only when $E \ll \frac{m_l}{m_h}\Delta_{so}$. In addition, such a model cannot describe Auger transitions at all, since the basis states of the carriers in different bands are orthogonal. The same applies to the spectrum in the SO band.

The Fourier amplitudes of the wave functions of both light and SO holes can be represented as (see equation (6)):

$$\Psi = \mathbf{k}f + \frac{i\delta}{E+\delta+\frac{\hbar^2k^2(E)}{2m_h}}[\mathbf{k}\times\boldsymbol{\sigma}f],$$

$$\Psi_s = -\frac{\hbar\gamma k^2(E)}{E_g+\delta-E}f, \tag{12}$$

where f is an arbitrary spinor related to the previously introduced function ϕ by the expression $\phi = k^2(E)f$.

The third solution in (6), which is related to heavy holes, satisfies the condition $\operatorname{div}\Psi = 0$ (as a result, $\Psi_s = 0$) and $\boldsymbol{\sigma}\operatorname{rot}\Psi = 0$. This follows from (8), because if $\phi = 0$, then $\eta = 0$ and vice versa. It is easy to see that

$$[\boldsymbol{\sigma}\times\Psi_h] = -i\Psi_h.$$

Thus, the law of dispersion describing the spectrum of heavy holes is as follows:

$$E_h = \delta - \frac{\hbar^2k_h^2}{2m_h}. \tag{13}$$

The components of the wave function of heavy holes must satisfy the equations:

$$\begin{cases}\Psi_{z\downarrow} = (\Psi_{x\uparrow} + i\Psi_{y\uparrow})\\ \Psi_{z\uparrow} = (-\Psi_{x\downarrow} + i\Psi_{y\downarrow})\end{cases} \Leftrightarrow\ [\boldsymbol{\sigma}\times\Psi] = -i\Psi, \tag{14}$$

$$\begin{cases}k_z\Psi_{z\uparrow} + k_x\Psi_{x\uparrow} + k_y\Psi_{y\uparrow} = 0\\ k_z\Psi_{z\downarrow} + k_x\Psi_{x\downarrow} + k_y\Psi_{y\downarrow} = 0\end{cases} \Leftrightarrow\ \operatorname{div}\Psi = 0. \tag{15}$$

Explicit expressions for the wave functions of holes can be obtained by solving these equations. They are given in *Appendix* II for quantum wells.

Electronic states

In principle, the conventional equations for electrons have the same form as for holes. Since the point Γ in the conduction band is degenerated only twice and the crystal field does not lead to additional splitting, there is no need to retain terms with parameters $\widetilde{\gamma}_i$. In addition, the presence of these terms in the equations for electrons is an excess of accuracy. Thus, a simplified model is valid for electrons:

$$\begin{cases}(E_c - E)\Psi_s - i\hbar\gamma\nabla\Psi = 0,\\ (E_v - \delta - E)\Psi - i\hbar\gamma\nabla\Psi_s + i\delta[\boldsymbol{\sigma}\times\Psi] = 0.\end{cases} \tag{16}$$

It is convenient to measure the electron energy from the lower edge of the conduction band ($E_c = 0$). Let us denote this energy as $\mathscr{E}$, so as not to confuse it with the total energy of the electron E, calculated from the same level as the energy of the holes. By introducing the functions ϕ and η into (16) in the same form as before (see equation (7)), we obtain

$$-(E_g+\delta+\mathscr{E})\phi + \frac{\hbar^2\gamma^2}{\mathscr{E}}\Delta\phi + i\delta\eta = 0,$$

$$-(E_g+\mathscr{E}+2\delta)\eta - 2i\delta\phi = 0. \tag{17}$$

Turning to the Fourier transforms, we find the law of dispersion for electrons

$$k^2 = \frac{\mathscr{E}}{\hbar^2\gamma^2}\frac{\mathscr{E}^2 + \mathscr{E}(2E_g+3\delta) + (E_g+3\delta)E_g}{E_g+\mathscr{E}+2\delta}. \tag{18}$$

If $\mathscr{E} \ll E_g$, δ, then the energy depends on the square of the wave vector:

$$\mathscr{E} = \frac{\hbar^2k^2}{2m_c}, \tag{19}$$

where

$$m_c^{-1} = 2\gamma^2\frac{E_g+2\delta}{(E_g+3\delta)E_g}.$$

The Fourier amplitude of the wave function for electrons is

$$\Psi_s = f,\quad \Psi = \frac{\mathscr{E}}{\hbar\gamma k^2(\mathscr{E})}\left[\mathbf{k}f + \frac{i\delta}{\mathscr{E}+E_g+2\delta}[\mathbf{k}\times(\boldsymbol{\sigma}f)]\right], \tag{20}$$

where f is an arbitrary spinor (see (12)).

3.1.2. Probability flux and equations near the heterogeneous border

The expression for the probability flux can be derived from the equation (5) by substituting $E \to -i\hbar\frac{\partial}{\partial t}$, and then using a procedure similar to that used in quantum mechanics [24]. It can also be obtained by the **kp**-method in the 2nd order of perturbation theory. As a result, for the probability flux in the case of holes, we obtain the following expression:

$$\mathbf{j}_h = \frac{E_g+\delta-E}{2m_l\gamma}[\Psi_s\Psi^* + \Psi_s^*\Psi] - \frac{i\hbar}{2m_h}(\Psi\times\operatorname{rot}\Psi^* - \Psi^*\times\operatorname{rot}\Psi). \tag{21}$$

For electrons in the conduction band, this expression has a simpler form

$$\mathbf{j}_e = \gamma[\Psi_s\Psi^* + \Psi_s^*\Psi]. \tag{22}$$

The question of boundary conditions for wave functions is still open. Approximate methods for solving this problem have been developed in recent years [19]. We will use the approximation $\gamma = \text{const}$, which is a good approximation for semiconductor heterostructures based on compounds $A^{III}B^{V}$ [19].

The discrepancy between the parameter γ in the quantum well and the barrier region results in a slight change in the Auger coefficient. Using the method developed in Ref. [21]

and assuming continuity of the Kane parameter, we obtain from the system (5) Kane equations that can be integrated through a heterobarrier:

$$\begin{cases} (E_g + \delta - E)\Psi_s - i\hbar\gamma\nabla\boldsymbol{\Psi} = 0, \\ -E\boldsymbol{\Psi} - i\hbar\gamma\nabla\Psi_s + \dfrac{\hbar^2}{2m}\nabla[6\tilde{\gamma}_2\nabla\boldsymbol{\Psi}] \\ + \dfrac{\hbar^2}{2m}\dfrac{\partial}{\partial x_k}(\tilde{\gamma}_1 - 2\tilde{\gamma}_2)\dfrac{\partial}{\partial x_k}\boldsymbol{\Psi} + i\delta[\boldsymbol{\sigma}\times\boldsymbol{\Psi}] = 0. \end{cases} \quad (23)$$

Using these equations and the law of conservation of probability flux density, we obtain boundary conditions for the envelopes of wave functions (see *Appendix* II).

3.1.3. Carrier states in a quantum well

The wave functions in a quantum well can be found using the symmetry properties of the Hamiltonian. Without taking into account the spin, the Hamiltonian $\mathscr{H}_0$ is invariant in case of the substitution $x \to -x$. Let us consider the operator $\mathscr{R}$, such that

$$\mathscr{R}: (x, y, z) \to (-x, y, z), \quad \mathscr{R} = \mathscr{I}C_{\pi x}, \quad (24)$$

$$\mathscr{H}_0\mathscr{R} = \mathscr{R}\mathscr{H}_0,$$

where $\mathscr{I}$ is the inversion operator, and $C_{\pi x}$ is the rotation operator by an angle π relative to the axis x perpendicular to the plane of the quantum well.

Taking into account the spin-orbit interaction, the Hamiltonian can be written as

$$\mathscr{H} = \mathscr{H}_0 + \frac{\hbar}{4m^2c^2}[\nabla V \times \mathbf{p}]\boldsymbol{\sigma}, \quad (25)$$

where $\mathbf{p}$ is the momentum operator and V is the potential energy of an electron in the crystal. The last term does not commute with $\mathscr{R}$. Therefore, the symmetry operator $\mathscr{D}$ can be found as the product of the operator $\mathscr{R}$ and some spin matrix S, i.e. $\mathscr{D} = \mathscr{R} \otimes S$. Since the inversion leaves the sign of the vector product unchanged, the matrix S must satisfy the relations

$$\begin{cases} S\sigma_x = \sigma_x S \\ S\sigma_y = -\sigma_y S \\ S\sigma_z = -\sigma_z S \end{cases},$$

$$\sigma_x = \begin{bmatrix} 0 & 1 \\ 1 & 0 \end{bmatrix}, \ \sigma_y = \begin{bmatrix} 0 & -i \\ i & 0 \end{bmatrix}, \ \sigma_z = \begin{bmatrix} 1 & 0 \\ 0 & -1 \end{bmatrix}. \quad (26)$$

Obviously, the Pauli spin matrix S may be taken for the matrix σ_x: $S = \sigma_x$.

The functions $\Psi(x, y, z)$ and $\mathscr{D}\Psi(-x, y, z)$ satisfy the same equation. Therefore, the eigenfunctions of the Hamiltonian can be searched for as eigenfunctions of the operator $\mathscr{D}$:

$$\Psi(x, y, z) = \nu\,\mathscr{D}\Psi(-x, y, z), \quad (27)$$

where $\nu = \pm 1$. The values $\nu = \pm 1$ correspond to states of carriers with different symmetries. With this choice of wave functions, the boundary conditions can be satisfied only on one heterogeneous boundary, since they will be satisfied automatically on the other. By solving equation (27), we find the necessary conditions for the various components of the symmetrized wave function:

$$\Psi_{s\uparrow}(x, y, z) = \pm\Psi_{s\downarrow}(-x, y, z),$$

$$\Psi_{x\uparrow}(x, y, z) = \mp\Psi_{x\downarrow}(-x, y, z),$$

$$\Psi_{y\uparrow}(x, y, z) = \pm\Psi_{y\downarrow}(-x, y, z),$$

$$\Psi_{z\uparrow}(x, y, z) = \pm\Psi_{z\downarrow}(-x, y, z),$$

where „+“ corresponds to $\nu = 1$, and „–“ corresponds to $\nu = -1$ for components s, y, z and vice versa for the component x. The corresponding expressions for the components of the wave functions of electrons and holes are given in *Appendix* II.

3.2. Matrix element of Auger recombination

The probability of Auger recombination per unit time is calculated in terms of the 1st order perturbation theory in electron-electron interaction:

$$W_{i\to f} = \frac{2\pi}{\hbar}|M_{fi}|^2\delta(\varepsilon_f - \varepsilon_i), \quad (28)$$

where

$$M_{fi} = \langle\Psi_f(\boldsymbol{r}_1, \boldsymbol{r}_2, \nu_1, \nu_2)\left|\frac{e^2}{\kappa_0|\boldsymbol{r}_1 - \boldsymbol{r}_2|} + \tilde{\Phi}(\mathbf{r}_1, \mathbf{r}_2)\right| \times \Psi_i(\boldsymbol{r}_1, \boldsymbol{r}_2, \nu_1, \nu_2)\rangle \quad (29)$$

— matrix element of the electron-electron interaction, $\boldsymbol{r}_1$ and $\boldsymbol{r}_2$ — carrier coordinates, ν_1 and ν_2 — spin variables (see (27)), $\tilde{\Phi}(\mathbf{r}_1, \mathbf{r}_2)$ — additional potential arising from the difference in the dielectric constants of the quantum well and the barrier. The explicit expression for $\tilde{\Phi}(\mathbf{r}_1, \mathbf{r}_2)$ is given in *Appendix* III.

Taking into account the antisymmetrization of wave functions, the matrix element of the Auger transition can be represented as

$$M_{fi} = M_{\mathrm{I}} - M_{\mathrm{II}}, \quad (30)$$

where

$$M_{\mathrm{I}} = \langle\Psi_3(\boldsymbol{r}_1, \nu_1)\Psi_4(\boldsymbol{r}_2, \nu_2)\left|\frac{e^2}{\kappa_0|\boldsymbol{r}_1 - \boldsymbol{r}_2|} + \tilde{\Phi}(\mathbf{r}_1, \mathbf{r}_2)\right| \times \Psi_1(\boldsymbol{r}_1, \nu_1)\Psi_2(\boldsymbol{r}_2, \nu_2)\rangle. \quad (31)$$

The expression for M_{II} can be obtained from (31) by replacing the indices 1 and 2 in the wave functions Ψ_1 and Ψ_2. Next, the indexes I and II in the expressions for matrix elements will be omitted. Here M_{I} is a direct Coulomb matrix element, and M_{II} is an exchange element.

We will consider two Auger recombination processes, CHCC and CHHS, since they actually determine the Auger recombination rate. Strictly speaking, this terminology is inapplicable to a quantum well, since there is a mixing of subbands of heavy holes, light holes, and SO holes. However, as noted above, in the case of $m_c \ll m_h$, the degree of mixing between heavy and light holes is small, and the mixing of SO holes with heavy and light holes at $\Delta_{so} \gg T$ is negligible. The latter condition is almost always fulfilled for semiconductors $A^{III}B^{V}$. Therefore, we can use the terminology given above.

The estimation of matrix elements for Auger processes CHCC and CHHS is similar. For simplicity, later in this section we will mainly consider the matrix elements of Auger transitions of CHCC. However, in the next section, approximate expressions for the Auger coefficient will be given for both the CHCC and the CHHS processes. The matrix element of the electron-electron Coulomb interaction is most conveniently calculated using the Fourier representation. We will take into account that the wave functions of the carriers in the quantum well are plane waves in the longitudinal direction (see *Appendix* II):

$$\Psi_i(\mathbf{r}) = \psi_i(x, \mathbf{q}_i)e^{i\mathbf{q}_i\boldsymbol{\rho}},$$

where $\mathbf{q}$ and $\boldsymbol{\rho}$ are the longitudinal component of the wave vector and the longitudinal coordinate, respectively. Explicit expressions for the wave functions of electrons and holes ψ_i are given in *Appendix* II. Then

$$M = \frac{4\pi e^2}{\kappa_0}\frac{1}{2q}\int\limits_{-\infty}^{\infty}\int\limits_{-a/2}^{a/2}\psi_4^*(x_1)\psi_3^*(x_2) \times \left(e^{-q|x_1-x_2|} + \tilde{\phi}(x_1, x_2, q)\right)\psi_1(x_1)\psi_2(x_2)\, dx_1 dx_2, \tag{32}$$

$q = |\mathbf{q}_1 - \mathbf{q}_4| = |\mathbf{q}_3 - \mathbf{q}_2|$ is the momentum transmitted in the plane of the quantum well during the Coulomb interaction, a is the width of the quantum well, $\tilde{\phi}$, the expression for which is given in *Appendix* III, corresponds to the potential $\tilde{\Phi}$. The integration over x_2 is limited to the region of the quantum well due to the fact that heavy holes, due to their relatively large mass, are usually strictly localized inside the well. Here x and $\boldsymbol{\rho}$ denote the coordinates orthogonal and parallel to the planes of the quantum well, $\mathbf{q}$ and k denote the longitudinal and x-components of the quasi-momentum of particles.

As can be seen from equation (32), Auger scattering occurs on a one-dimensional exponentially decreasing potential, which depends on the transverse transmitted momentum. The state of an excited particle can be in both a continuous and a discrete spectrum, and the latter option occurs when the longitudinal momentum of the particle significantly exceeds the transverse momentum. (As usual, we assume that $(V_c, V_v) < E_g$). When determining the Auger recombination rate, both localized and delocalized states should be considered as the final states of an excited particle. The probability of an electron (hole) transition to a localized or free state leads to the existence of various Auger recombination mechanisms in quantum wells.

3.2.1. Calculation of the Auger recombination matrix element for transitions of an excited particle into a continuous spectrum

Let's use the approximation $V_c, V_v \ll E_g$ to calculate the matrix element. Obviously, this approximation also assumes that $k_4^2 + q^2 \gg k_1^2$, i. e., the total momentum of the excited electron significantly exceeds that of the localized electron. The integral along the coordinate x_1 can be calculated by integration by parts. Here n-th antiderivative of the function $\psi_4 e^{-qx}$ is equal to:

$$F_4^n(q, x) = (-1)^n \frac{(e^{qx}\psi_4(x))^{(n)}}{(k_4^2 + q^2)^n} e^{-2qx}.$$

Then we get an approximate expression for the matrix element M_1:

$$M \approx M^{(1)} + M^{(2)}, \tag{33}$$

where

$$M^{(1)} = -\frac{4\pi e^2}{\kappa_0(q^2 + k_4^2)}\left(\mathscr{F}(a/2)\int\limits_{-a/2}^{a/2} e^{qx_2}\psi_3^*(x_2)\psi_2(x_2)dx_2 - \mathscr{F}(-a/2)\int\limits_{-a/2}^{a/2} e^{-qx_2}\psi_3^*(x_2)\psi_2(x_2)dx_2\right). \tag{34}$$

Here

$$\mathscr{F}(a/2) = e^{-qa/2}\psi_{4s}^*(a/2)\psi_{1s}(a/2) \times \left(\frac{3V_c + V_v}{4E_g} - \frac{\kappa_0 - \tilde{\kappa}_0}{\kappa_0 + \tilde{\kappa}_0}\right). \tag{35}$$

The index s in ψ_{4s} and ψ_{1s} means that only the sth component of the wave function is taken, $\tilde{\kappa}_0$ is the dielectric constant in the barrier region.

$$M^{(2)} = \frac{4\pi e^2}{\kappa_0(q^2 + k_4^2)}\int\limits_{-a/2}^{a/2}\psi_4^*(x)\psi_3^*(x)\psi_2(x)\psi_1(x)dx. \tag{36}$$

It should be noted that since wave functions are spinors, the components ψ_4^* should be multiplied by the components ψ_1, and vice versa, the components ψ_3^* should be multiplied by the components ψ_2.

Thus, it turns out that the matrix element AR splits into two parts. The first of them $M^{(1)}$ is associated with the presence of heteroboundaries, and the second $M^{(2)}$ corresponds to short-range Coulomb scattering. The latter is easy to understand, since during the Auger transition, a large momentum is transferred from a localized electron to

an excited one, and this is possible only if the scattering particles are very close to each other. It should be noted that both $M^{(1)}$ and $M^{(2)}$ and, accordingly, the matrix element M itself are actually thresholdless matrix elements. Indeed, they are not subject to any restrictions imposed on the initial carrier momenta k_1, k_c, k_h by the quasi-momentum conservation laws. However, the mechanisms leading to the non-conservation of the quasi-momentum $k_1 + k_2 \neq k_3 + k_4$ in the components $M^{(1)}$ and $M^{(2)}$ are different. In $M^{(1)}$, nonconservation is associated with carrier scattering at heterogeneous boundaries, and the same mechanism leads to the appearance of a thresholdless Auger process during scattering on a single heterobarrier [13]. In $M^{(2)}$, the reason for the violation of the conservation law is the limitation of the volume of integration over x by the region of the quantum well, which leads to the appearance of a function of the $\frac{\sin(ka/2)}{k}$ type instead of δ-function $\delta(k)$. Substituting (35) into (34), and integrating over x_2, we have

$$M^{(1)} \approx \frac{8\pi e^2}{\kappa_0(q^2+k_4^2)(q^2+k_3^2)}\left(\frac{3V_c+V_v}{4E_g}-\frac{\kappa_0-\tilde{\kappa}_0}{\kappa_0+\tilde{\kappa}_0}\right) \times (\psi_4^*(a/2)\psi_1(a/2))\,(\psi_3^*(a/2)\psi_2(a/2))'\,(1\pm e^{-qa}). \tag{37}$$

The sign $\pm$ in the last brackets is selected according to the parity of the product $\psi_3^*(x)\psi_2(x)$, the sign „+“ corresponds to an even product, and the sign „–“ corresponds to an odd one. In the case of $qa \gg 1$, this exponent can be ignored, and the matrix element $M^{(1)}$ corresponds to an independent scattering on two heterogeneous boundaries. The term $(\kappa_0 - \tilde{\kappa}_0)/(\kappa_0 + \tilde{\kappa}_0)$ in equation (37) arises from taking into account the additional potential $\tilde{\Phi}(\mathbf{r}_1, \mathbf{r}_2)$ (see equation (31)). It should be noted that the matrix element $M^{(1)}$ is zero if the parities in the products $\psi_3^*(x)\psi_2(x)$ and $\psi_4^*(x)\psi_1(x)$ are different.

Let's move on to the analysis of $M^{(2)}$. The integral included in $M^{(2)}$ is proportional to the sum

$$\int_0^a \psi_4^*(x)\psi_3^*(x)\psi_1(x)\psi_2(x)\,dx \propto \sum \pm \frac{\sin(k_4-k)a/2}{k_4-k}, \tag{38}$$

where k runs through eight different values of $k = \pm k_1 \pm k_2 \pm k_3$. Of all the terms in the sum (38), the largest is the one for which $k = k_1 + k_2 + k_3$. The reason is that this term has the lowest threshold energy. By threshold energy, we mean the average energy of a heavy hole involved in the Auger transition. The contribution to the sum from the other terms is less significant, and for simplicity we will ignore it. Then the expression for the matrix element for the quasi-threshold Auger process takes the following form:

$$M^{(2)} \approx \frac{\pi e^2}{\kappa_0(q^2+k_4^2)}\,e^{i\delta}\,\frac{\hbar\gamma}{E_g}\,\frac{1+2/3\alpha}{1+\alpha}\,A_cA_fA_cA_h \times \frac{\sin(k_f-k_{c1}-k_{c2}-k_h)a/2}{k_f-k_{c1}-k_{c2}-k_h} \times \begin{cases} q_hk_ce^{i\phi_{2,3}}+q_ck_h, & \nu_c=\pm\nu_h, \\ q_cq_h\sin\phi_{2,3}, & \nu_c=\mp\nu_h. \end{cases} \tag{39}$$

Here δ is an insignificant phase multiplier, A_i denotes the normalization constant, ν_c and ν_h are spin indices introduced according to (27), $\phi_{2,3}$ is the angle between the transverse momentum of the electron and the hole. As follows from (39), in the limit $a \to \infty$, the matrix element $M^{(2)}$ becomes proportional to $\delta(k_f - k_1 - k_2 - k_h)$, and therefore tends to the matrix element for the bulk case. On the contrary, $M^{(1)}$ tends to zero in the limit of $a \to \infty$. Therefore, we call $M^{(1)}$ and $M^{(2)}$ thresholdless and quasi-threshold processes, respectively.

3.2.2. Calculation of the Auger recombination matrix element for transitions of an excited carrier into a discrete spectrum

Let us now turn to the analysis of the matrix element of Auger transitions in which a high-energy particle remains in a bound state ψ_4. This case corresponds to the approximation $q_4 \gg k_4$. The matrix element can be calculated in the same way as above for $M^{(2)}$:

$$M^{(3)} \approx \frac{4\pi e^2}{\kappa_0(q^2+k_4^2)}\int_{-a/2}^{a/2}(\psi_4^*\psi_1)(\psi_3^*\psi_2)\,dx. \tag{40}$$

This integral is easy to calculate; however, the general formula is very cumbersome and will not be given here. We will only make an estimate $M^{(3)}$, which is valid in the case when the carriers are in the ground quantum state. Then we have

$$M^{(3)} \approx \frac{1}{q^2+k_4^2}\,e^{i\delta}\,\frac{\hbar\gamma}{Z} \times A_cA_fA_cA_ha/2\alpha q_cq_h\sin\phi_{2,3} \quad (\nu_c=-\nu_h). \tag{41}$$

Here $\phi_{2,3}$ is the angle between the transverse components of the quasi-momentum of an electron and a heavy hole and α is a multiplier of the order of unity resulting from integrating the product of the envelopes of the carrier wave functions in the quantum well region:

$$\int_0^{a/2} f_1f_2f_3f_4\,dx \approx a/2\alpha, \tag{42}$$

where $f_i = \cos k_i x$, i numerates the initial and final states of the particles involved in the Auger recombination process.

It should be noted that α is nonzero only if the parities of the pairwise products $\Psi_1\Psi_4$ and $\Psi_c\Psi_h$ coincide. For wide quantum wells, when particles can be in various bound quantum states, α transforms into into the expression

$$\alpha = \frac{1}{16} \sum_{\nu_1,\nu_2,\nu_3,\nu_4=0,1} (-1)^{\nu_i\sigma_i} \frac{\sin\left((-1)^{\nu_i} k_i a/2\right)}{(-1)^{\nu_i} k_i a/2}. \qquad (43)$$

This implies summation by index i from 1 to 4, σ_i characterizes the parity of the function f_i ($\sigma_i = 1$ for an odd function and $\sigma_i = 0$ for an even one).

3.3. Auger recombination coefficient

To calculate the Auger recombination rate, it is necessary to sum the probability of Auger transition per unit of time (28) for all initial and final states of the carriers with the corresponding weights — occupation numbers.

$$G = \frac{2\pi}{\hbar} \sum_{\mathbf{k}_1,\mathbf{k}_2,\mathbf{k}_3,\mathbf{k}_4} \langle M^2\rangle \cdot f_1 f_2 (1-f_3)(1-f_4) \times \delta(E_3 + E_4 - E_1 - E_2). \qquad (44)$$

Here f_1 and f_2 are the Fermi carrier distribution functions in the initial state, and f_3 and f_4 are the Fermi carrier distribution functions in the final state,

$$\langle M^2\rangle = \sum_{\nu_1,\nu_2,\nu_3,\nu_4} |M_{fi}|^2$$

is the square of the matrix element, summed over the spins of the particles in the initial and final states. For highly excited states, the distribution function f_4 can be set to zero. It should be noted that instead of $1 - f_3$, we can write $\widetilde{f_3}$, where $\widetilde{f_3}$ is the distribution function for carriers of the opposite sign: holes for the CHCC process and electrons for the CHHS process.

The contributions to the Auger recombination rate from the matrix elements $M^{(1)}$ $M^{(2)}$ and $M^{(3)}$ can be separated, since the excited particle in such processes lies in different quantum states. The matrix elements $M^{(1)}$ and $M^{(2)}$, on the one hand, and $M^{(3)}$, on the other hand, describe transitions in which an excited particle occupies states in a continuous and discrete spectrum, respectively. It is more difficult to separate the contributions from $M^{(1)}$ and $M^{(2)}$. Although the physical difference between them remains, however, there is a term describing the interference between them. For small values of the width of the quantum well, interference is significant, since both processes are virtually thresholdless; however, even if this interference is ignored, we still get the correct result in the order of magnitude, reflecting all the main features of the Auger recombination coefficient as a function of temperature and parameters of the quantum well structure.

For a sufficiently wide quantum well, the interference between $M^{(1)}$ and $M^{(2)}$ can be ignored. Indeed, if $M^{(1)}$ has no singularities as a function of quasi-momenta, then $M^{(2)}$ has a maximum modulo at $k_4(q) + k_3 = k_1 + k_2$. With the width of the quantum well tending to infinity, the maximum at this point has the character of a δ-function. As the thickness of the quantum well decreases, the maxima of these probabilities approach each other and the area of overlap between these matrix elements increases.

The Auger recombination probabilities for the CHCC process corresponding to the matrix elements $M^{(1)}$ and $M^{(2)}$ are shown in Figure 3 depending on the longitudinal momentum of the heavy hole at different widths of the quantum well. It can be seen from the figure that interference between the thresholdless process corresponding to $M^{(1)}$ and the quasi-threshold process corresponding to $M^{(2)}$, in accordance with the above, occurs only in narrow quantum wells. It should be noted that the AR probabilities are fairly smooth functions of the longitudinal momentum of a heavy hole, since their calculation was based on summation over discrete quantum states of carriers. At q, close to the maximum value determined by the law of conservation of longitudinal momentum and energy, the probability of RR has a root divergence, eliminated by integration over q, i.e., when calculating the Auger recombination rate. The probability of Auger transitions for the CHHS process has the form similar to the expression for the CHCC process.

In accordance with the above, we will represent the Auger recombination rate as

$$G = G_1 + G_2 + G_3, \qquad (45)$$

where the rate G_1 corresponds to a thresholdless AR channel with a matrix element $M^{(1)}$, the rate G_2 corresponds to a quasi-threshold AR channel with a matrix element $M^{(2)}$ and the rate G_3 is the threshold channel of the AR with the matrix element $M^{(3)}$.

The expressions for the rates G_1 and G_2 can be obtained using the formula (44), replacing the summation over k_4 with integration and moving from δ-function based on energy to δ-function based on momentum. Further, we will study the Auger recombination coefficient C, which is related to the rate G by the ratio

$$G = Cn^2p \quad \text{and} \quad G = Cp^2n$$

for CHCC and CHHS Auger processes, respectively. Here n and p denote two-dimensional concentrations of electrons and holes, respectively. We have the following for the CHCC thresholdless process

$$C_1 \approx \frac{32\pi^2 e^4}{\kappa_0^2} \frac{\hbar\gamma^2}{E_g^3} \frac{F(\Delta_{so}/E_g)}{a(a+2/\kappa_c)^2} \frac{k_c^2\kappa_c^2}{(k_c^2+\kappa_c^2)^2} \frac{V_c}{E_g} \times \left(\frac{3V_c + V_v}{4E_g} - \frac{\kappa_0 - \tilde{\kappa}_0}{\kappa_0 + \tilde{\kappa}_0}\right)^2 \left\langle \frac{q_h^2 k_h^2}{(q_h^2+k_h^2)^3} \frac{1}{k_4(q_h)} \right\rangle, \qquad (46)$$

where

$$F(x) = \left(\frac{1+2x/3}{1+x}\right)^2 \frac{1+7x/9+x^2/6}{(1+x/2)(1+4x/9)}$$

— a coefficient of the order of one, $x = \Delta_{so}/E_g$.

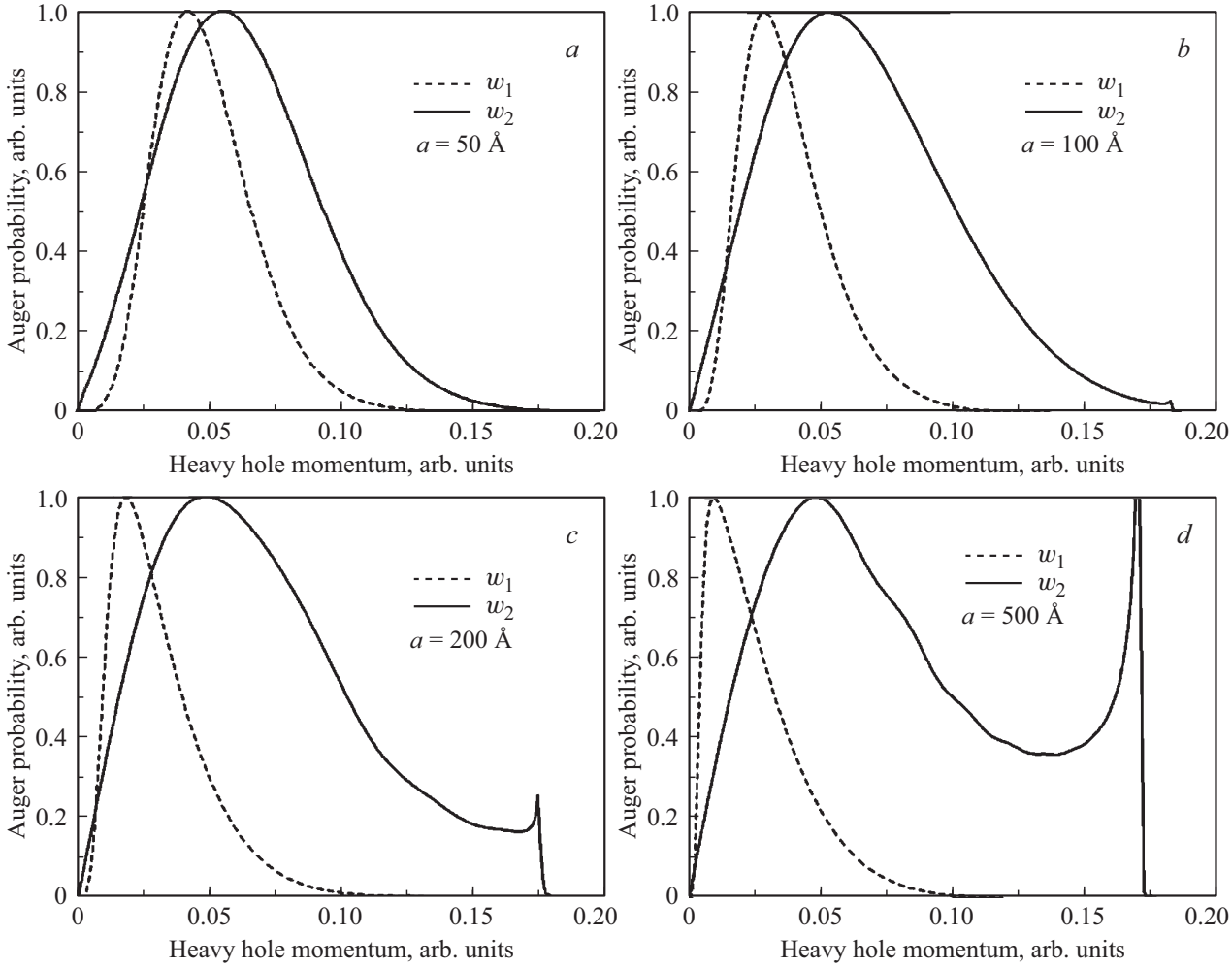

Figure 3. Auger transition probabilities w_1 and w_2 corresponding to thresholdless and quasi-threshold matrix elements $M^{(1)}$ and $M^{(2)}$, depending on the longitudinal momentum of the heavy hole at $T = 300$ K for different quantum well widths a, Å: a — 50, b — 100, c — 200, d — 500.

It should be noted that if the Kane parameter γ is discontinuous, then to the term in (46)

$$\left(\frac{3V_c + V_v}{4E_g} - \frac{\kappa_0 - \tilde{\kappa}_0}{\kappa_0 + \tilde{\kappa}_0}\right)^2$$

the expression should be added

$$\frac{E_{0c}}{2E_g}\left(\frac{\delta\gamma}{\gamma}\right)^2,$$

where E_{0c} is the energy of dimensional quantization for the electron and $\delta\gamma = \gamma - \tilde{\gamma}$ is the difference between the Kane parameter in the quantum well and the barrier region. However, this additive is usually negligible. The angle brackets in (46) and below denote the averaging over the distribution function of heavy holes. In the case of the Boltzmann distribution, which is usually the case for holes, this averaging has the form

$$\langle f(q_h, k_h)\rangle = \frac{1}{Z}\sum_n \int_0^\infty q_h f(q_h, k_{hn}) e^{-\frac{k_{hn}^2 + q_h^2}{q_T^2}} dq_h,$$

where

$$Z = \frac{2}{q_T^2}\sum_n e^{-\frac{k_{hn}^2}{q_T^2}},$$

$q_T = \sqrt{2m_h T}/\hbar$ — thermal momentum of heavy holes, k_{hn} — wave vector corresponding to n-th level of dimensional quantization for heavy holes.

The following expression can be obtained for the CHHS thresholdless process: for C_1:

$$C_1 \approx \frac{2\pi^2 e^4}{\kappa_0^2 \hbar}\frac{V_c}{E_g}\frac{k_c^2\kappa_c^2}{(k_c^2+\kappa_c^2)^2}\frac{\tilde{F}(\Delta_{so}/E_g)}{a^2(a+2/\kappa_c)}\frac{\hbar^3}{m_{so}^3(E_g-\Delta_{so})^3} \times \left\langle \frac{k_{h1}^2 k_{h2}^2 q_{h1}^2 (q_{h1}^2 + q_{h2}^2)}{(q_{h1}^2 + k_{h1}^2)^3 (q_{h2}^2 + k_{h2}^2)} \right\rangle, \quad (47)$$

where

$$\tilde{F}(x) = \frac{(2x + 3(1-x)(1-m_{so}/m_h))^2}{2x^2 + (x + 3(1-x)(1-m_{so}/m_h))^2}\frac{1 + 2x/3}{1+x}.$$

The angle brackets in (47) denote the averaging over the distribution function of two heavy holes. When deducing (47), we assumed that $E_g - \Delta_{so} \gg m_h/m_{so}T$.

Similarly, for the quasi-threshold CHCC process, we obtain the following expression for C_2:

$$C_2 \approx \frac{\pi^2 e^4}{\kappa_0^2}\frac{\hbar^3\gamma^4}{E_g}\frac{F(\Delta_{so}/E_g)}{a(a+2/\kappa_c)^2} \times \left\langle \frac{q_c^2 k_h^2 + q_h^2(k_c^2+\frac{1}{2}q_c^2)}{(q_h^2+k_h^2)k_4(q_h)}\frac{1-\cos(k_f-k_h-2k_c)a}{2(k_f-k_h-2k_c)^2}\right\rangle. \quad (48)$$

The direct calculation of the Auger coefficient C_2 for the quasi-threshold CHHS process gives a cumbersome expression. The following is a simplified expression for sufficiently narrow quantum wells at $k_c \gg q_c$:

$$C_2 \approx \frac{\pi^2 e^4}{4\kappa_0^2}\frac{E_c}{E_g}\frac{\hbar^3}{m_{so}^2(E_g-\Delta)^3}\frac{\tilde{F}(\Delta_{so}/E_g)}{a^2(a+2/\kappa_c)} \times \left\langle \frac{1-\cos(k_{so}-k_{h1}-k_{h2}-k_c)a}{2(k_{so}-k_{h1}-k_{h2}-k_c)^2} \times \frac{q_{h2}^2\left((k_{so}^2+k_{h1}^2)q_{h1}^2+q_{h2}^2k_{h1}^2+2k_{h1}^2(\mathbf{q}_{h1}\mathbf{q}_{h2})+[\mathbf{q}_{h1}\times\mathbf{q}_{h2}]^2\right)}{(q_{h1}^2+k_{h1}^2)(q_{h2}^2+k_{h2}^2)k_{so}}\right\rangle. \quad (49)$$

Finally, for the CHCC threshold process, we have the following expression for C_3:

$$C_3 \approx \frac{32\pi^2 e^4}{\kappa_0^2\hbar E_g}\frac{a}{(a+1/\kappa_c)^3}\frac{1+\frac{7}{9}x+\frac{1}{6}x^2}{(1+x/3)^2}\frac{1+\frac{2}{3}x}{1+x} \times \left\langle \frac{q_{th}^2}{q_T^2}\frac{q_c^2}{(q_{th}^2+k_h^2)^3}e^{-\frac{q_{th}^2}{q_T^2}}\alpha^2\right\rangle_n. \quad (50)$$

Here α is the multiplier included in the expression (41). We average only over discrete quantum states of heavy holes in (50). The threshold momentum q_{th} is derived from the law of conservation of energy and the longitudinal component of the quasi-momentum:

$$E_f(\sqrt{k_f^2+q_{th}^2}) = E_g + \frac{\hbar^2(q_{th}^2+k_h^2)}{2m_h} + \frac{\hbar^2(k_{c1}^2+k_{c2}^2)}{2m_c}.$$

For simplicity, here we have neglected the longitudinal momenta of electrons in determining the threshold energy due to their smallness. However, we take into account the energy of dimensional quantization of electrons, since it changes the effective band gap in the quantum well. If we expand the energy of the excited electron E_f into a series in terms ofmomenta near $q_{th} = Q$, where Q is the value of the electron momentum corresponding to the energy equal to E_g $\left(Q \approx \sqrt{\frac{4m_cE_g}{\hbar^2}}\right)$, then we can obtain the following estimate for threshold momentum values:

$$q_{th} \approx \sqrt{\frac{4m_cE_g}{\hbar^2} + \frac{3}{2}\left(k_c^2 + \frac{m_c}{m_h}k_h^2\right)}. \quad (51)$$

If the width of the quantum well tends to infinity, then the threshold momentum tends to its bulk value [10]. In addition, it should be borne in mind that for wide quantum wells with a large number of levels, the introduced multiplier α (see (43)) tends to δ, a function expressing the conservation law of the transverse component of the quasi-momentum:

$$\alpha^2 \longrightarrow \frac{\pi}{128}a\sum\delta(k_h \pm k_{c1} \pm k_{c2} \pm k_{c4}).$$

For narrow quantum wells, the threshold energy for the CHCC process increases (see (51)), and the Auger recombination coefficient C_3 (50) decreases by a factor compared to the bulk value

$$\exp\left(\frac{3k_c^2}{2q_T^2}\right) \approx \exp\left(\frac{3m_c}{2m_h}\frac{E_{0c}}{T}\right).$$

It is easy to estimate the characteristic width of the quantum well, for which this effect becomes significant, from the condition that the exponent is unity:

$$E_{0c} \approx T\frac{2m_h}{3m_c} \Leftrightarrow a \approx \pi\frac{1}{q_T}. \quad (52)$$

Thus, for quantum well widths a smaller than several reciprocal thermal momenta $a \lesssim \pi/q_T$, the threshold energy $E_{th}^3(a)$ becomes significantly higher than the bulk value E_{th}^{3D} (see Figure 4). For semiconductor compounds $A^{III}B^{V}$ at room temperature, equality (52) is achieved at the width of the quantum well ~ 100 Å.

For the CHHS threshold process, the momenta of heavy holes are not determined by threshold conditions and therefore it is necessary to perform integration with respect to them. At the same time, it turns out to be impossible to obtain an accurate analytical expression for the Auger coefficient C_3 for the CHHS process due to the fact that the matrix element M_3 is very cumbersome. However, it is easy to obtain an approximate expression by factoring out the averaged squared matrix element from the integrand sign:

$$C_3 \approx \frac{2\pi}{\hbar}\langle M_3^2\rangle\frac{1}{2\pi^2q_T^4}\int q_{h1}dq_{h1}q_{h2}dq_{h2}d\phi_{h1}d\phi_{h2}e^{-\frac{q_{h1}^2+q_{h2}^2}{q_T^2}} \times \delta\left(\tilde{E}_g - \Delta - \frac{\hbar^2(\mathbf{q_{h1}}+\mathbf{q_{h2}})^2}{2m_{so}} + \frac{\hbar^2q_{h1}^2}{2m_h} + \frac{\hbar^2q_{h2}^2}{2m_h}\right). \quad (53)$$

Here $\tilde{E}_g = E_g + E_{0e} + 2E_{0h} - E_{0\,so}$, where E_{0e}, E_{0h} $E_{0\,so}$ are the dimensional quantization energies for electrons, holes, and SO holes, respectively. Let's introduce a threshold momentum, setting it equal to

$$Q_{th}^2 = \frac{2(\tilde{E}_g - \Delta_{so})m_{so}}{\hbar^2(2-\mu_{so})},$$

where $\mu_{so} = m_{so}/m_h$. Then the expression for C_3 takes the form

$$C_3 \approx \frac{2m_{so}}{\hbar^3Q_{th}^2}e^{-\frac{Q_{th}^2}{q_T^2}}\langle M_3^2\rangle. \quad (54)$$

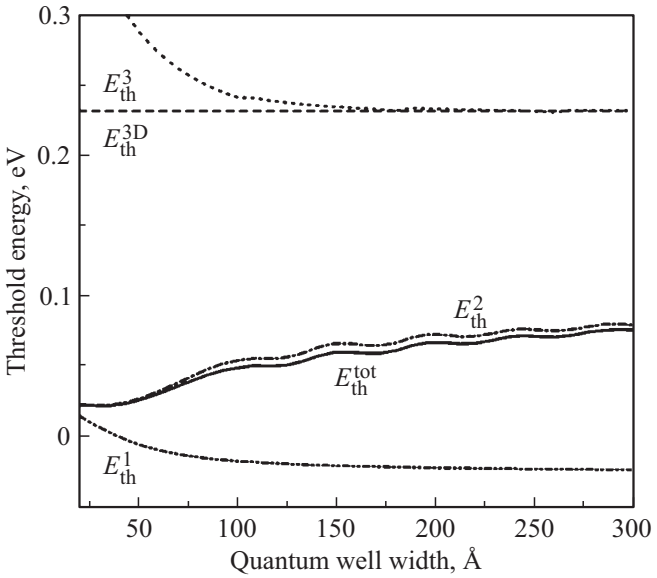

Figure 4. The dependence of the threshold energy for the CHCC process on the width of the quantum well for three Auger recombination mechanisms: thresholdless (E_{th}^1), quasi-threshold (E_{th}^2) and threshold (E_{th}^3) at $T = 300$ K. The solid curve corresponds to the threshold energy $E_{\text{th}}^{\text{tot}}$ for the total Auger recombination coefficient $C = C_1 + C_2$. The horizontal dotted line corresponds to the threshold energy E_{th}^{3D} for the three-dimensional Auger process.

Considering that $Q_{\text{th}} \gg k_{\text{so}}$, we obtain

$$C_3 \approx \frac{256 m_{\text{so}} \pi^2 e^4}{\hbar^3 \kappa_0^2} \frac{Q_{\text{th}}^2}{(Q_{\text{th}}^2 + 2k_h^2)^4} \times \frac{V_c}{E_g} \frac{k_c^2}{k_c^2 + \kappa_c^2} \frac{(1-\lambda_{\text{so}})^2}{1+2\lambda_{\text{so}}^2} \tilde{\alpha}^2 e^{-\frac{Q_{\text{th}}^2}{q_T^2}}, \quad (55)$$

where $\tilde{\alpha}$ is the multiplier defined as in the case of the CHCC process (see (41)), λ_{so} is derived from the expression for λ_l (see (175)) by substituting k_{so} instead of k_l.

Let's take a closer look at the Auger recombination coefficient C_2 for the quasi-threshold CHCC process. A replacement is possible for $a \longrightarrow \infty$ in the averaged function in (48):

$$\frac{1-\cos(k_f - k_h - 2k_c)a}{2(k_f - k_h - 2k_c)^2} \longrightarrow \frac{\pi a}{2} \delta(k_f - k_h - 2k_c). \quad (56)$$

This formula clearly shows the presence of a threshold in this limit due to the law of conservation of quasi-momentum, and the coefficient C_2 after multiplication by a^2 becomes a three-dimensional expression. For comparison, we present the result of the study in Ref. [10] for C_{3D} and our limiting expression:

$$C_{3D} = 6\sqrt{2\pi^5} \frac{e^4 m_c \hbar^3}{\kappa_0^2} \frac{1}{E_g^{5/2} T^{1/2} m_c^{1/2} m_h^{3/2}} e^{-\frac{2m_c}{m_h}\frac{E_g}{T}}, \quad (57)$$

$$C_2 \cdot a^2 = 6 \frac{16\sqrt{2\pi^5}}{27} \frac{e^4 m_c \hbar^3}{\kappa_0^2} \frac{1}{E_g^{5/2} T^{1/2} m_c^{1/2} m_h^{3/2}} e^{-\frac{2m_c}{m_h}\frac{E_g}{T}}. \quad (58)$$

The 4 multiplier in (58) arises from the fact that when calculating M_2 according to (39), it is necessary to take into account not only the summand with $k = k_{c1} + k_{c_2} + k_h$, but also the summands with $k = k_{c1} - k_{c_2} + k_h$, $k = -k_{c1} + k_{c_2} + k_h$, and $k = -k_{c1} - k_{c_2} + k_h$. As the width of the quantum well tends to infinity, all four terms give the equal contribution to C_2. As can be seen, the difference between expressions (57) and (58) is only in the numerical factor. A small discrepancy of $\approx 2/3$ times is due to the fact that in the presence of a large number of electronic levels, it is necessary to distinguish the momenta of dimensional quantization of electrons among themselves, $k_{c1} \neq k_{c2}$. In addition, the expression (57) was obtained for a simplified model when the magnitude of the spin-orbit splitting is assumed to be infinitely large. The condition $\Delta_{\text{so}} \leq E_g$ was used for the derivation of (58), which is fulfilled for the majority of narrow-band semiconductors $A^{III}B^{V}$. When calculating (58), we neglected the value of V_c compared to E_g.

In the general case, $C_2 a^2$ instead of $(C_2 + C_3)a^2$ should be used, and the expression (58) will remain valid. However, the limiting transition from a quasi-threshold to a threshold process (see (56)) can be realized only for very wide quantum wells. A qualitative criterion for this transition can be obtained from analyzing the probability of the Auger transition as a function of the momentum of a heavy hole. As noted above, a quasi-threshold process with a coefficient C_2 dominates in wide quantum wells. The probability of this process has two characteristic extremes (see 48)). The first one corresponds to the maximum of the square of the transition matrix element near the threshold value of the momentum of the heavy hole. The width of this maximum is of the order of the inverse width of the quantum well. The second one lies near the value of the thermal momentum of the hole q_T. Then

$$C_2 \approx C_2^{\text{th}}(Q_h \approx q_{\text{th}}) + C_2^T(Q_h \approx q_T), \quad (59)$$

where Q_h is the value of the momentum of the heavy hole: $Q_h^2 = k_h^2 + q_h^2$;

$$\frac{C_2^T}{C_2^{\text{th}}} \approx \frac{\lambda_{E_g}}{a} \left(\frac{T}{E_{\text{th}}}\right)^{3/2} e^{\frac{E_{\text{th}}}{T}}. \quad (60)$$

Here $\lambda_{E_g} \approx 2\pi/q_{\text{th}}$ is the characteristic wavelength of an electron with energy close to E_g. From a comparison of the terms C_2^{th} and C_2^T, we can obtain a criterion for the transition of a quasi-threshold AR process into a three-dimensional threshold process:

$$a \gg a_c,$$

where

$$a_c = \lambda_{E_g} \left(\frac{T}{E_{\text{th}}}\right)^{3/2} \exp\left(\frac{E_{\text{th}}}{T}\right). \quad (61)$$

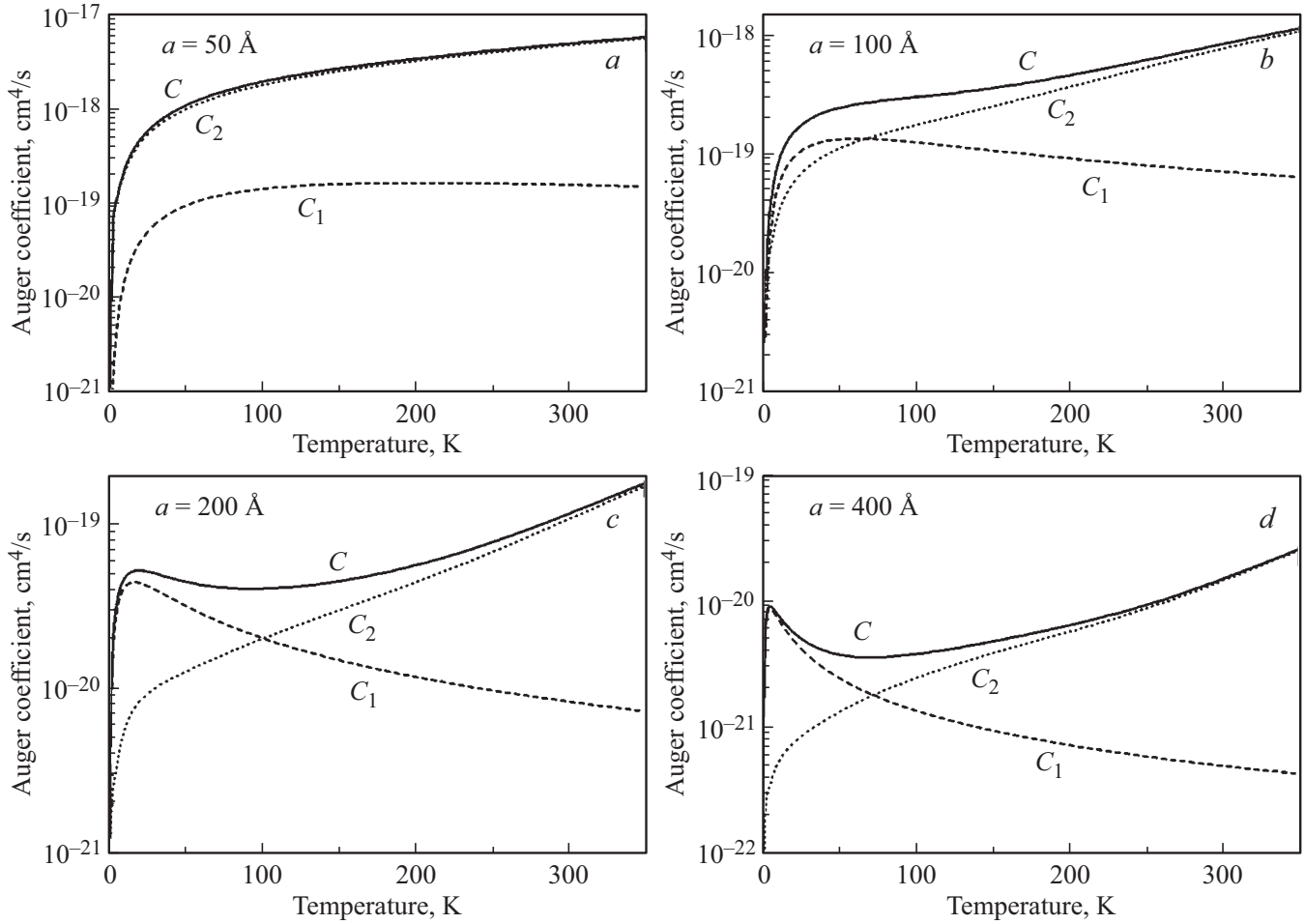

Figure 5. Temperature dependences of the total Auger coefficient and partial contributions of thresholdless and quasi-threshold mechanisms at different widths of the quantum well.

For semiconductors with a band gap of ~ 1 eV at room temperature, the critical thickness (a_c) can reach several thousand angstroms. However, the value a_c is significantly greater than the free path of carriers in semiconductors. This clearly shows that the correct calculation of the Auger coefficient in homogeneous semiconductors should include interparticle scattering processes if the critical width a_c exceeds the mean free path of the carriers (see *Appendix* I).

As the width of the quantum well decreases, the maximum probability w_2 as a function of the momentum of heavy holes shifts to the long-wavelength side (see Figure 3). This leads to a decrease in the threshold energy of this process and, as a result, to a weakening of the temperature dependence of the Auger-recombination coefficient.

Figure 4 shows the dependences of the threshold energy for the CHCC process on the width of the quantum well for all three Auger recombination mechanisms C_1, C_2 and C_3 separately and for the total Auger recombination process $C = C_1 + C_2 + C_3$, defined by the formula

$$E_{\text{th}}^{i}(T) = T^2 \frac{d \ln C_i}{dT}, \quad i = 1, 2, 3. \tag{62}$$

The threshold energy for a quasi-threshold process is less than its three-dimensional value, since the value of the critical thickness $a_c \approx 1000$ Å is greater than the maximum width of the quantum well (see Figure 4). For the thresholdless Auger process, the threshold energy decreases with increasing width of the quantum well and becomes negative at a certain thickness. This behavior of the threshold energy is due to the fact that for sufficiently wide quantum wells, the Auger recombination coefficient C_1 becomes a decreasing function of temperature (see Figure 5). As the width of the quantum well increases, the threshold energy for the total Auger process tends to its limiting value $E_{\text{th}}^{\text{3D}}$, indicated in Figure 4.

Let's turn to the consideration of the thresholdless Auger process. As noted above, the probability of a thresholdless Auger transition has no extrema as a function of the momentum of a heavy hole. Therefore, the coefficient C_1 has a weak non-exponential temperature dependence. This was first studied in detail in Ref. [13]. In addition, the function $C_1(T)$ is non-monotonic and has a maximum. The presence of such a maximum is easy to explain. At low temperatures and, consequently, low longitudinal

momenta of the carriers, their wave functions are almost orthogonal and the value of C_1 is small. As the temperature increases, the characteristic momentum transmitted during the Coulomb interaction increases (it is approximately equal to the thermal momentum of a heavy hole). Therefore, at low temperatures, the Auger coefficient is an increasing function of temperature. With a further increase in temperature, the Auger recombination coefficient $C_1(T)$ reaches a maximum and begins to decrease, since the Coulomb long-range interaction responsible for the Auger process is small for large transmitted momenta.

The temperature at which the AR coefficient has a maximum can be easily estimated from considerations of the equality of the energy of dimensional quantization of holes to the temperature $T \approx \hbar^2\pi^2/2m_h a^2$. It should be noted that this maximum would not exist if we considered the overlap integral I_{th} proportional to the transmitted momentum. In our opinion, this approximation, which is used for most of the structures studied, is an unjustified assumption, although it is often used in the literature (see, for example, [25], and leads to incorrect expressions for the Auger recombination rate and its incorrect dependences on temperature and quantum well parameters.

The Auger coefficient C_1 has a very sharp dependence on the width of the quantum well a. For wide quantum wells, even after multiplying by a^2, $C_1 a^2$ remains a decreasing function of the width of the quantum well. Therefore, such a process can be predominant only for sufficiently narrow quantum wells. At $a \approx 1/k_c$, the coefficient C_1 has a maximum associated with a weak overlap of the wave functions of the charge carriers. With a further decrease in the width of the quantum well, the rate of the thresholdless Auger process gradually decreases due to a decrease in the overlap of the wave functions of electrons and holes. A similar expression for C_1 for the CHCC process was obtained in Refs. [15,16].

Figure 6 shows the dependences of the Auger recombination coefficients C_1 and C_2 on the width of the quantum well at different temperatures for a model structure based on the InGaAsP compound. It can be seen that all curves exhibit a pronounced peak. The positions of these peaks for C_1 and C_2 are practically independent of temperature. The peak for the threshold process (C_3) is reached at higher quantum well widths than for quasi-threshold and thresholdless processes, and its position shifts with increasing temperature. This is primarily due to a decrease in the threshold energy for the threshold process with an increase in the width of the quantum well (see Figure 4), rather than the overlap factor of the wave functions.

Figure 5 shows the temperature dependence of the total Auger recombination coefficient and the partial contributions of thresholdless and quasi-threshold mechanisms for different quantum well widths. It can be seen from this figure that the thresholdless Auger process prevails at low temperatures ($C_1 > C_2$) for sufficiently wide quantum

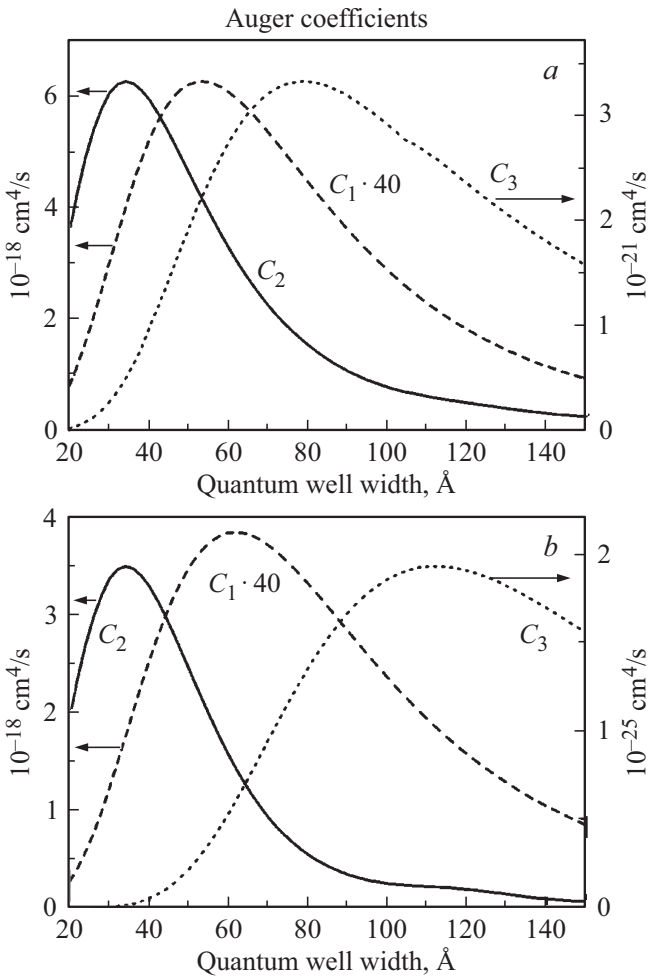

Figure 6. Auger coefficients C_1, C_2 and C_3 for thresholdless, quasi-threshold and threshold processes depending on the width of the quantum well at different temperatures T, K: a — 150, b — 300.

wells, and at high temperatures, on the contrary, the quasi-threshold process becomes larger ($C_2 > C_1$). Therefore, the dependence of the total Auger recombination coefficient on temperature has a characteristic form with a maximum and a minimum. As the width of the quantum well increases, both the maximum and minimum of the Auger recombination coefficient shift towards low temperatures and disappear at the limit of a quantum well of infinite width. Thus, in the case of a homogeneous semiconductor, the Auger recombination coefficient is a monotonic function of temperature. It should be noted that the Boltzmann distribution of carriers was used to calculate the temperature dependence of the Auger recombination coefficients. At low temperatures, electrons and holes, as a rule, obey Fermi-Dirac statistics. Consequently, the average momenta of electrons and holes involved in the Auger process are weakly temperature-dependent. As a result, the Auger recombination coefficient has a smoother dependence on temperature and does not vanish at $T \to 0$.

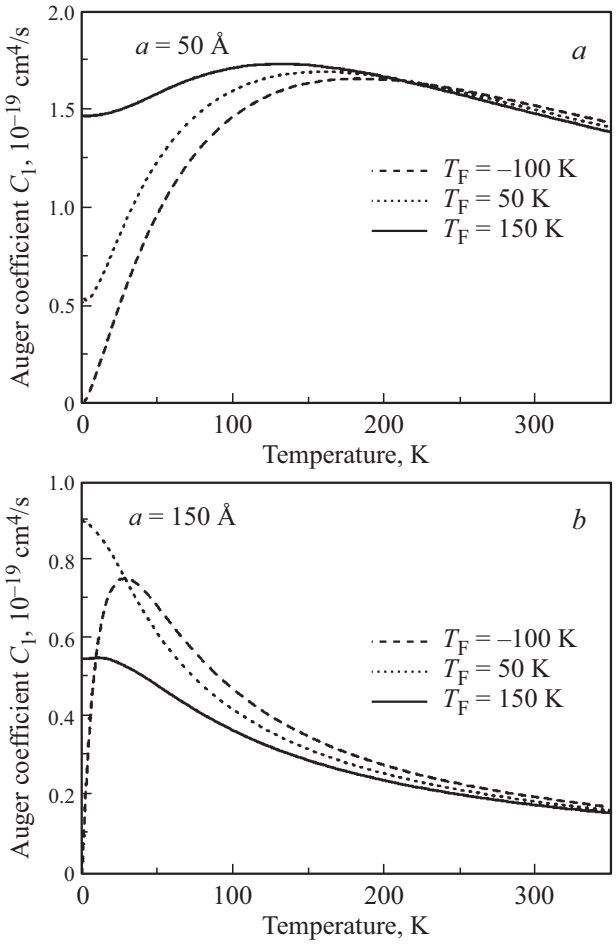

Figure 7. Comparison of the dependence of the threshold Auger recombination coefficient C_1 on temperature at different values of the Fermi energy of holes for two different values of the width of the quantum well a, Å: a — 50, b — 150. T_F in the figure denotes the Fermi energy expressed in Kelvins The curve with $T_F = -100$ K approximately corresponds to the Boltzmann statistics.

Figure 7 shows the dependence of the thresholdless Auger recombination coefficient C_1 on temperature at different values of the Fermi energy of holes for quantum wells of different widths. Significant differences between the Auger-recombination coefficients for the Fermi-Dirac and Boltzmann distributions exist in the case of $T \ll E_F$, where E_F is the Fermi energy of holes. This condition is usually realized only in the case of very low temperatures, at which the Auger -recombination process is not relevant.

3.4. Phonon-assisted Auger recombination process in quantum wells

At high temperatures in homogeneous semiconductors, the threshold Auger recombination process prevails ($C^{3D} \propto e^{-\frac{E_{th}}{T}}$). However, at a sufficiently low temperature, such a process becomes exponentially weak. In this case, the Auger recombination rate is no longer determined by the scattering of two electrons (two holes). The mechanisms leading to the elimination of the threshold should be considered. It is believed that the main mechanism of this kind is the emission and absorption of a virtual optical phonon. Due to the transfer of a large momentum to the phonon, the AR threshold for heavy holes is removed and the rate of such an Auger process is a power function of temperature [26–28]. The probability of Auger recombination involving phonons is calculated in the 2nd order of perturbation theory for electron-electron (hole-hole) and electron-phonon (hole-phonon) interactions [29].

For quantum wells, the situation is very different from the bulk case, even in the 1st order of perturbation theory due to the presence of a thresholdless process. Therefore, it is *a priori* obvious that the conditions under which the phonon-assiated Auger process in a quantum well dominates the phononless one strongly depend on the width of the quantum well.

As already noted, there are three Auger recombination processes in the quantum well: threshold, quasi-threshold, and thresholdless. The Auger recombination coefficient for a phonon-assiated threshold process is quite easily calculated when the following conditions are met [28]:

$$E_g \gg 2\mu E_g \gg \hbar\omega_{lo}, \tag{63}$$

where ω_{lo} is the frequency of the optical phonon, $\mu = m_e/m_h$. It can be shown that the coefficient of the phonon-assisted Auger process is expressed in terms of the previously calculated for the direct process (50) as follows:

$$C_{ph}^3 \approx C_3 \frac{e^2\hbar\omega_{lo}}{2\overline{\kappa}a}\frac{T}{E_{th}^{2D}}\, g(a, k_{th})\, \frac{1}{e^{\frac{\hbar\omega_{lo}}{T}} - 1} \times \left[\frac{e^{\frac{\hbar\omega_{lo}}{T}}}{\left(E_{th}^{2D} - \hbar\omega_{lo}\right)^2} + \frac{1}{\left(E_{th}^{2D} + \hbar\omega_{lo}\right)^2}\right] e^{E_{th}^{2D}/T}, \tag{64}$$

where $\overline{\kappa} = \frac{\kappa_0\kappa_\infty}{\kappa_0 - \kappa_\infty}$; κ_∞ is a high-frequency permittivity of the medium; $g(a, k_{th})$ is a multiplier reflecting the two-dimensional nature of holes in a quantum well [30]:

$$g(a, k_{th}) = k_{th}^2 a^2 \left[\frac{1}{2k_{th}^2 a^2} + \frac{1}{4(\pi^2 + k_{th}^2 a^2)}\right] \times \left[1 - \frac{1 - e^{-2k_{th}a}}{2k_{th}a}\frac{2\pi^4}{(\pi^2 + k_{th}^2 a^2)(2\pi^2 + 3k_{th}^2 a^2)}\right]. \tag{65}$$

For comparison, it is convenient to give the corresponding three-dimensional expression for the phonon-assiated Auger recombination coefficient:

$$C_{ph}^{3D} \approx C^{3D}\frac{e^2\hbar\omega_{lo}}{2\sqrt{\pi\overline{\kappa}}}\left(\frac{T}{E_{th}^{3D}}\right)^{3/2}\frac{k_{th}}{e^{\hbar\omega_{lo}/T} - 1} \times \left[\frac{e^{\frac{\hbar\omega_{lo}}{T}}}{\left(E_{th}^{3D} - \hbar\omega_{lo}\right)^2} + \frac{1}{\left(E_{th}^{3D} + \hbar\omega_{lo}\right)^2}\right] e^{E_{th}^{3D}/T}. \tag{66}$$

The calculation results for two-dimensional and three-dimensional phonon-assiated Auger recombination processes with threshold matrix elements of electron-electron interaction are very similar. A significant difference for narrow quantum wells is an increase in the threshold energy $E_{\text{th}}^{\text{2D}}$ due to the presence of levels of dimensional quantization of charge carriers (51). Accordingly, the criterion for the predominance of the phonon-assiated Auger recombination process (C_{ph}^{3}) over the phononless threshold Auger process (C_3) in quantum wells is performed at slightly higher temperatures than in the three-dimensional case. However, as noted above, the threshold Auger process in narrow quantum wells is itself several orders of magnitude weaker than the thresholdless and quasi-threshold processes [$C_3 \ll (C_1,\ C_2)$]. Therefore, the phonon-assiated AR process with a threshold matrix element of electron-electron interaction (M_{ee}) also cannot compete with thresholdless and quasi-threshold processes [$C_{\text{ph}}^{3} \ll (C_1 C_2)$].

Let us now consider the phonon-assiated Auger process with a thresholdless matrix element ($M_{ee} = M^{(1)} + M^{(2)}$) for the CHCC process. For simplicity, we will use the approximation of conservation of momentum when scattering a hole on an optical phonon [31]. In this case, the state of the virtual hole is fixed and the following expression can be obtained for the probability of phonon-assiated Auger recombination:

$$w_{i\to f} = \pm \frac{2\pi}{\hbar} \sum_s \frac{|M_{ee}|^2 |M_{\text{ph}}|^2}{(E_s \mp \hbar\omega_{LO} - E_h)^2} \frac{e^{\pm\frac{\hbar\omega_{LO}}{T}}}{e^{\pm\frac{\hbar\omega_{LO}}{T}} - 1} \times \delta(E_i - E_f) d\nu_f, \tag{67}$$

where E_s is the energy of the virtual heavy hole, M_{ph} is the matrix element of the scattering of the virtual hole on an optical phonon; signs „+“ and „−“ correspond to the processes of phonon emission and absorption, respectively. It is easy to see that there is a singularity in the expression (67) when the denominator is equal to zero. To eliminate this divergence, it is necessary to take into account transitions not to stationary, but to quasi-stationary states of a heavy hole, i. e., to states with complex energy. In this case, the pole at (67) will move into the region of complex energies, then the probability is proportional to the denominator:

$$w_{i\to f} \propto \frac{1}{(E_s \mp \hbar\omega_{LO} - E_h)^2 + \Gamma^2},$$

where $\Gamma = \hbar/\tau$. The characteristic lifetimes τ corresponding to these states can vary widely depending on temperature, concentration of free carriers, etc. It makes sense to consider a resonant phonon-assiated process in the 2nd order of perturbation theory only when the half-width of quasi-stationary hole and phonon states is less than the energy of the optical phonon ($\hbar\omega_{\text{lo}}$). Otherwise, it is necessary to calculate the Auger coefficient in the 1st order of perturbation theory using the Lorentz function

$$f(\Delta E) = \frac{1}{\pi} \frac{\Gamma}{\Delta E^2 + \Gamma^2}$$

instead of the δ-function expressing the law of conservation of energy. For the phonon-assisted Auger recombination process with a quasi-threshold electron-electron interaction matrix element, both resonant and virtual Auger processes are possible, with the former prevailing in the case of narrow quantum wells, and the latter in the case of sufficiently wide wells.

In the general case, the Auger coefficient for a phonon-assisted process can be represented as

$$C_{\text{ph}} = C_{\text{ph}}^{1} + C_{\text{ph}}^{2}, \tag{68}$$

where

$$C_{\text{ph}}^{1,2} = \pm \frac{\pi\omega e^2}{\overline{\kappa} Z} \frac{\exp(\pm\hbar\omega_{\text{lo}}/k_{\text{B}}T)}{\exp(\pm\hbar\omega_{\text{lo}}/k_{\text{B}}T) - 1} \times \sum_{m,n,\nu_n} \int \frac{d^2Q}{(2\pi)^2} \frac{d^2q_h}{(2\pi)^2} \left(\frac{\partial E_4}{\partial k_4}\right)^{-1} \times \frac{|M_{ee}(n, \nu_n, \mathbf{q}_h) + \mathbf{Q}|^2}{\left(\frac{\hbar^2(m^2-n^2)\pi^2}{2a^2 m_h^2} - \frac{\hbar^2(\mathbf{q}_h+\mathbf{Q})^2}{2m_h} + \frac{\hbar^2 q_h^2}{2m_h} \pm \hbar\omega_{\text{lo}}\right)^2 + \Gamma^2} \times J_{n,m}(Q) f_h(m, q_h). \tag{69}$$

Here:

$$Z = \sum_m \int \frac{dq_h}{(2\pi)^2} f_h(m, \mathbf{q}_h),$$

$$J_{n,m}(Q) \approx \frac{a}{2} \times \frac{(1+\delta_{m,n})[(m+n)^2\pi^2 + Q^2a^2] + (m-n)^2\pi^2 + Q^2a^2}{[(m+n)^2\pi^2 + Q^2a^2][(m-n)^2\pi^2 + Q^2a^2]},$$

$f(m, q_h)$ is hole distribution function at the m-th quantum level.

The function $J_{n,m}(Q)$ was calculated in Ref. [31] for a non-degenerate zone. In the case of phonon scattering by heavy holes, its magnitude will be somewhat smaller. However, this circumstance is not essential for our purposes. In (69), as the momenta of bound electrons, their average thermal momenta must be substituted into the matrix element of the electron-electron interaction. The Auger coefficients C_{ph}^{1} (sign „+“) and C_{ph}^{2} (sign „−“) correspond to the processes of phonon emission and absorption, respectively. Regardless of the form of the matrix element of the Coulomb interaction, the phonon-assisted Auger process is thresholdless. This corresponds to the fact that the main contribution to the Auger coefficient C_{ph} is made by hole momenta, which are of the order of magnitude equal to thermal momenta. Therefore, when calculating C_{ph}, its average thermal value can be substituted as the longitudinal momentum of the hole q_h.

The expression (69) is easy to analyze if the temperature is much lower than the energy of optical phonons. In this case, the thermal momentum of the holes q_h can be neglected in comparison with the phonon momentum Q, which is approximately equal to the momentum of the virtual hole. It is easy to see that the Auger transition

probability as a function of Q has two extrema. The first one corresponds to the minimum of the denominator at (69) and the resonant transition. It should be noted that for the process associated with phonon absorption, no such a feature is observed and the resonant process does not occur. The second extremum corresponds to the maximum of the square of the matrix element and, as a rule, corresponds to the virtual Auger transition. With sufficiently wide quantum wells, the matrix element of the electron-electron interaction as a function of the momentum of a heavy hole has a form close to the δ-function. In this case, the second extremum prevails, and the phonon scattering process is virtual. As the width of the quantum well decreases, the δ-function broadens for a quasi-threshold matrix element and, in addition, the role of a thresholdless matrix element weakly dependent on Q increases. This leads to an increase in the resonant Auger transition and a weakening of the virtual one. For narrow quantum wells, the matrix element of the Coulomb electron-electron interaction weakly depends on Q, therefore, the resonance process is dominant for them. As can be shown, in this case, the following estimate of the value of the Auger recombination coefficient for the phonon-assisted Auger process is valid:

$$C_{\text{ph}} \approx \frac{\omega_{\text{lo}} e^2 m_h a}{8\tilde{\kappa}\hbar\Gamma} J_{1,1}(Q_0) \frac{2\pi}{\hbar} \frac{3k(E_g)}{4E_g} |M_{ee}(Q_0)|^2, \quad (70)$$

where $Q_0 = \sqrt{\frac{2m_h\omega_{\text{lo}}}{\hbar}}$. It immediately follows that the ratio of the phonon-assisted Auger recombination coefficient to the phononless one has the form:

$$\frac{C_{\text{ph}}}{C} \approx \frac{\Gamma_{\text{ph}}}{\Gamma} \frac{(M_{ee}(Q_O))^2}{(M_{ee}(q_T))^2}, \quad (71)$$

where $C = C_1 + C_2$ is the Auger coefficient for the direct Auger process, $\Gamma_{\text{ph}} = \hbar/\tau_{\text{ph}}$, τ_{ph} is the hole scattering time on an optical phonon, q_T is the hole thermal momentum.

It can be seen that the phonon-assisted Auger process can dominate the phononless process only when the values of Γ_{ph} and Γ are close, or in the case of extremely low temperatures, when the ratio of matrix elements taken at momenta Q_0 and q_T is high. It should be noted that at high concentrations of nonequilibrium carriers, when the Auger recombination process generally becomes significant, hole-hole scattering, as a rule, turns out to be a much more effective relaxation mechanism than hole-phonon scattering. This leads to the fact that the ratio $\Gamma_{\text{ph}}/\Gamma$ turns out to be small and the phononless Auger recombination process prevails over the phonon-assisted process up to very low temperatures. Figure 8 shows the dependence of the phonon-assisted Auger transition coefficient as a function of temperature at different quantum well widths. The assumed half-width Γ is 20 meV, a characteristic value corresponding to hole-hole scattering.

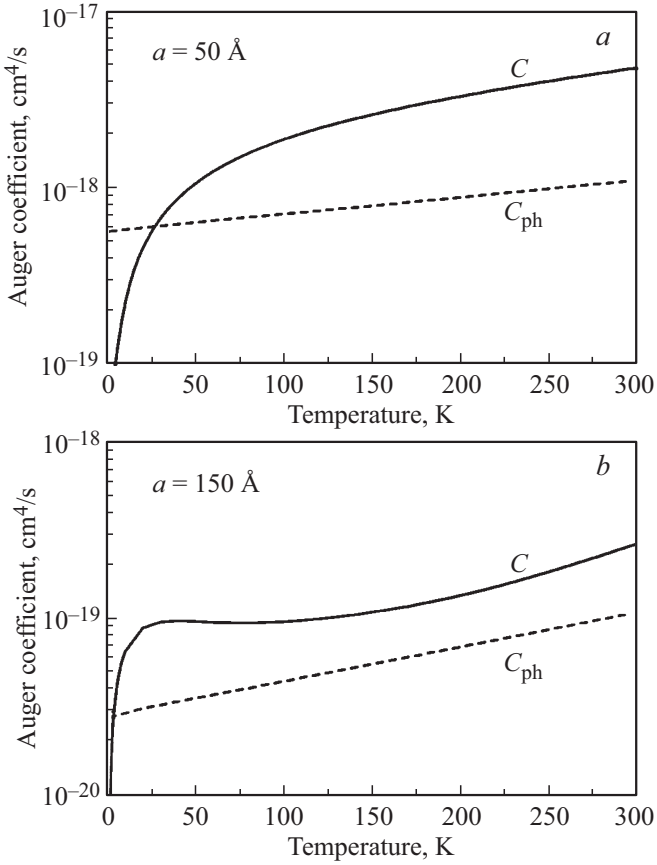

Figure 8. Dependence of Auger recombination coefficients for direct thresholdless C and phonon-assisted C_{ph} processes on temperature at different quantum well widths.

3.5. Discussion of the results

Our analysis has shown that there are three different Auger recombination mechanisms for CHCC and CHHS Auger recombination processes in semiconductor structures with quantum wells: thresholdless, quasi-threshold, and threshold. The first of them is weakly dependent on temperature. The effective threshold energy for the second process significantly depends on the width of the quantum well (see Figure 4). Namely, it tends to zero for substantially narrow quantum wells and approaches the bulk value in the limit $a \to \infty$. Therefore, there are no clear differences between thresholdless and quasi-threshold AR mechanisms in narrow quantum wells, and they can be considered as one thresholdless AR process. The third, threshold, AR process is similar to that which takes place in bulk semiconductors. The only difference is that its threshold energy is slightly higher than in a bulk semiconductor due to an increase in the effective band gap (51). The rate of the threshold process is low in narrow quantum wells compared to the rates of the first two processes G_1 and G_2. Quasi-threshold and threshold Auger processes merge at the limit $a \to a_c$ and form a process of bulk Auger recombination $C_2a^2 + C_3a^2 \to C^{3D}$. The critical QW

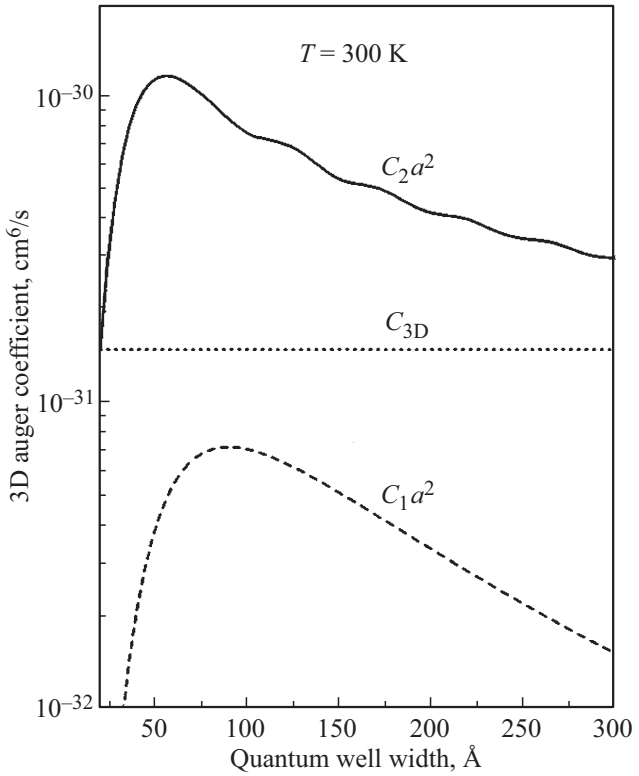

Figure 9. The dependence of the three-dimensional (3D) values of Auger coefficients C_1a^2 and C_2a^2 on the width of the quantum well at $T = 300$ K. The horizontal line corresponds to the bulk Auger coefficient C_{3D}.

width strongly (exponentially) depends on temperature and can reach several hundred angstroms at room temperature for a semiconductor with $E_g \approx 1$ eV. The rate of the thresholdless process tends to zero during the transition to a bulk semiconductor. For narrow QWs, the two-dimensional Auger coefficient multiplied by a^2 exceeds the value for the bulk Auger process due to the dominance of thresholdless and quasi-threshold processes (Figure 9). Thus, the Auger recombination process in quantum wells turns out to be enhanced compared to a homogeneous semiconductor. This gain is all the more significant at low temperatures. It should be noted that the entire analysis of the dependences of Auger recombination coefficients (C_1, C_2, C_3) on temperature and quantum well parameters is qualitatively applicable equally to CHCC and CHHS Auger processes. However, since we did not specify the model structures with quantum wells, we illustrated these dependencies using the example of the CHCC process.

It should be noted that significant suppression of Auger recombination processes in quantum wells is possible under the conditions $(V_c, V_v) > E_g$ and $E_2 - E_1 > E_g$ (E_1 and E_2 are the energies of the first and second levels of dimensional quantization of carriers) [32]; i. e., in the case when the energy of the excited particle is insufficient to transition to a continuous spectrum or to the next level of dimensional quantization. To fulfill these conditions, it is necessary to create structures with deep and narrow quantum wells for both electrons and holes. Current technologies allow the creation of such structures based on materials InAs/AlSb [33] and InAs/GaSb/AlSb [34]. In such deep quantum wells, there is only a threshold Auger recombination process corresponding to the coefficient C_3. This coefficient can be several orders of magnitude smaller than the Auger coefficients for thresholdless and quasi-threshold processes (C_1, C_2) in shallow quantum wells $\left((V_c, V_v) < E_g\right)$.

It should also be noted that in the case of quantum wells, the phonon-assisted Auger recombination process also undergoes significant changes. Similarly to the phononless Auger recombination process, there are three different phonon process mechanisms (C^3_{ph}, C^2_{ph}, and C^1_{ph}) corresponding to threshold, quasi-threshold, and thresholdless matrix elements of electron-electron interaction. The first process is quite similar to the three-dimensional one. However, in the case of narrow quantum wells, this process is noticeably weaker than the thresholdless and threshold Auger recombination processes. In the literature, it is this phonon-assisted process that is considered the main process of Auger recombination in quantum wells [35,36]. Phonon-assisted Auger recombination processes with quasi-threshold and thresholdless matrix elements of electron-electron interaction can be resonant processes. At low temperatures, they can compete with phononless Auger recombination processes. However, due to the absence of a strong dependence of the latter on temperature, such competition is possible at much lower temperatures than in the three-dimensional case (see Figure 8). As the width of the quantum well increases, the resonant scattering by phonons weakens and we pass on to the usual three-dimensional conditions.

3.6. Conclusion

In conclusion, we will focus on some interesting recent papers devoted to the analysis of Auger recombination in narrow-gap materials.

A model has been developed in Ref. [37] for calculating the Auger recombination rate in narrow-gap quantum wells based on HgTe/CdHgTe heterostructures. It is shown that in order to correctly calculate the Auger recombination rate in such structures, it is necessary to take into account the processes of impact ionization and the effect of free charge carriers on the electron-electron interaction. It is shown that relaxation processes can both increase and decrease the Auger recombination rate depending on the carrier concentration. The dependences of the Auger recombination rate for quantum wells with a band gap of 35 and 50 meV at four temperatures of 8, 100, 200 and 300 K are presented.

The authors of Ref. [38] studied the effect of interface roughness on Auger recombination in quantum wells. They showed that as the ratio of surface roughness to the thickness of the quantum well increases, Auger recombination

increases significantly. In particular, when considering the realistic roughness of the interface for the InGaN quantum well, the increase in the Auger recombination rate compared to a quantum well with an ideal interface can be approximately 4 orders of magnitude.

The lifetime of nonequilibrium charge carriers in GaInN/GaN-based quantum wells is studied in Ref. [39]. It is shown that at high charge carrier densities, the lifetime of nonradiative recombination weakly depends on temperature and is proportional to the inverse of the density, which implies an excitonic, thresholdless Auger process.

The authors of Ref. [40] studied the internal quantum efficiency of quantum wells based on (In,Ga)N/GaN. Several mechanisms have been proposed to explain the decrease in quantum efficiency, including the Auger recombination, both internal and caused by defects. An atomistic model of the electronic structure was used within the framework of the strong coupling approximation to calculate the rates of radiative and Auger recombinations.

The authors of Ref. [41] based on a systematic study of the dependence of the threshold current density on temperature and hydrostatic pressure in combination with a theoretical analysis of the gain coefficient and threshold carrier density, determined the dependence of the Auger recombination coefficients on wavelength in InGaAsSb/GaSb quantum well lasers emitting in the wavelength range of $1.7-3.2\,\mu$m. The ratio of Auger recombination rates for the two processes CHCC and CHSH was analyzed.

A detailed theoretical analysis of nonradiative Auger recombination in narrow-gap quantum wells of mercury, cadmium and telluride (CdHgTe quantum wells) is proposed in Ref. [42]. A microscopic model is considered for calculating Auger recombination rates in quantum wells with different Cd fractions depending on the nonequilibrium carrier density, taking into account the complex band structure. However, the authors did not take into account the influence of spatial heterogeneity of the quantum structure on the AR mechanism.

The effect of Auger recombination processes on the temperature quenching of photoluminescence in HgTe/CdHgTe quantum wells is studied in Ref. [43]. It is assumed that the resonant thresholdless Auger process determines the threshold values of stimulated radiation over a wide temperature range.

From the analysis of the listed publications, it follows that the authors, when studying Auger recombination processes, do not take into account the influence of spatial heterogeneity of quantum heterostructures on Auger recombination mechanisms. However, as is well known, Auger recombination is a process of Coulomb interaction between particles. As noted above, the effect of the heterogeneous boundary on the Coulomb interaction between particles is fundamental: the heterogeneous boundary modifies the laws of conservation of energy and momentum, which leads to the formation of new Auger recombination channels. As shown in this review, for all types of quantum heterostructures (quantum wells, quantum filaments, and quantum dots), spatial heterogeneity affects both the Auger recombination mechanisms and the dependence of the Auger recombination rate on temperature and on the parameters of the quantum heterostructure, as well as the magnitude of the rate.

Conflict of interest

The authors of the review declare that there is no conflict of interest.

References

[1] V.N. Abakumov, V.I. Perel, I.N. Yassievich. *Bezyzluchatel'naya rekombinaciya v poluprovodnikah* (PIYAF im. B.P. Konstantinova, SPb., 1997). (in Russian).
[2] P.T. Landsberg. *Recombination in Semiconductors* (Cambridge University Press, 1991).
[3] P.V. Auger. C. R. Acad Sci.: Paris, **180**, 65 (1925).
[4] Z.N. Sokolova. *Teoriya mezhzonnoj ozhe-rekombinacii v pryamozonnyh poluprovodnikah*: avtoref. dis. kand. fiz.-mat. nauk (FTI im. A.F. Ioffe, L., 1982). (in Russian).
[5] A. Polkovnikov, G. Zegrya. Phys. Rev. B, **64** (7), 073205 (2001).
[6] G.G. Zegrya, V.I. Perel. *Osnovy fiziki poluprovodnikov* (Fizmatlit, M., 2009). (in Russian).
[7] A.R. Beattie, P.T. Landsberg. Proc. Roy. Soc., **A249** (1256), 16 (1959).
[8] M.P. Mikhailova, A.A. Rogachev, I.N. Yassievich. FTP, **10**, 1460 (1976). (in Russian).
[9] M.P. Mikhailova, A.A. Rogachev, I.N. Yassievich. FTP, **11**, 1882 (1977). (in Russian).
[10] B.L. Helmont. JETF, **75** (8), 536 (1978). (in Russian).
[11] R.I. Taylor, R.A. Abram. Semicond. Sci. Technol., **3** (9), 859 (1988).
[12] P. Roussignol, M. Kull, D. Ricard, F. de Rougemont, R. Frey, C. Flytzanis. Appl. Phys. Lett., **51** (23), 1882 (1987).
[13] G.G. Zegrya, V.A. Kharchenko. JETF, **101** (1), 327 (1992). (in Russian).
[14] R.I. Taylor, R.A. Abram, M.G. Burt, C. Smith. Semicond. Sci. Technol., **5** (1), 90 (1990).
[15] M.I. Dyakonov, V.Yu. Kachorovskii. Phys. Rev. B, **49** (24), 17130 (1994).
[16] G.G. Zegrya, A.D. Andreev, N.A. Gun'ko, E.V. Frolushkina. Proc. SPIE, 2399, 307 (1995).
[17] I.V. Kudryashov, G.G. Zegrya, V.P. Evtikhiev, V.E. Tokranov. in the collection: *Compound Semiconductors (ISCS-23) 23th Int. Phys. Conf.* (St. Peterburg, Russia, September 23–27 1996), **155**, Chap. 10, p. 795.
[18] E.O. Kane. J. Phys. Chem. Sol., **1**, 249 (1957).
[19] P.C. Sercel, K.J. Vahala. Phys. Rev. B, **42**, 3690 (1990).
[20] R.A. Suris. FTP, **20** (11), 2008 (1986). (in Russian).
[21] M.G. Burt. J. Phys.: Condens. Matter., **4**, 6651 (1992).
[22] B.A. Foreman. Phys. Rev. B, **49**, 1757 (1994).
[23] G.L. Bir, G.E. Pikus. *Simmetriya i deformatsionnye effekty v poluprovodnikakh*. (M., Nauka, 1972). (in Russian).
[24] L.D. Landau, E.M. Lifshitz. *Kvantovaya mekhanika. Nerelyativistkaya teoriya* (Nauka, M., 1989). (in Russian).
[25] H.L. Wang, M.J. Freeman, D.G. Steel, R. Craig, D.R. Scifres. Optics Lett., **18** (24), 2141 (1995).

[26] A. Haug. J. Phys. C: Solid State Phys., **16**, 4159 (1983).
[27] G.P. Agrawal, N.X. Dutta. *Long-Wavelength Semiconductor Lasers* (Van Nostrand Reinhold Company, N.Y., 1993).
[28] A. Haug. Appl. Phys. A, **51**, 354 (1990).
[29] A. Haug. J. Phys. Chem. Solids., **49** (6), 599 (1988).
[30] A.S. Polkovnikov, G.G. Zegrya. Phys. Rev. B, **58** (7), 4039 (1998).
[31] B.K. Ridley. J. Phys. C: Solid State Phys., **15** (28), 5899 (1982).
[32] G.G. Zegrya. In: *Antimonide-Related Strained-Layer Heterostructures*, (Gordon and Breach, Amsterdam, 1997) v. 3.
[33] S. Ideshita, A. Furukawa, Y. Mochizuki, M. Mizuta. Appl. Phys. Lett., **60** (20), 2549 (1992).
[34] M. Sweeny, J. Xu. Appl. Phys. Lett., **54**, 546 (1989).
[35] E.P. O'Reilly, M. Silver. Appl. Phys. Lett., **63** (24), 3318 (1993).
[36] E.P. O'Reilly, A.R. Adams. IEEE J. Quant. Electron., **30** (2), 366 (1994).
[37] V.Ya. Aleshkin, A.A. Dubinov, V.V. Rumyantsev. J. Appl. Phys., **138**, 135702 (2025).
[38] Chee-Keong Tan, Wei Sun, Jonathan J. Wierer jr., Nelson Tansu. AIP Advances, **7**, 035212 (2017).
[39] T. Langer, Al. Chernikov, D. Kalincev, M. Gerhard, H. Bremers, U. Rossow, M. Koch, A. Hangleiter. Appl. Phys. Lett., **103**, 202106 (2013).
[40] R.M. Barrett, J.M. McMahon, R. Ahumada-Lazo, J.A. Alanis, P. Parkinson, S. Schulz, M.J. Kappers, R.A. Oliver, D. Binks. ACS Photonics, **10**, 2632 (2023).
[41] T.D. Eales, I.P. Marko1, A.R. Adams, J.R. Meyer, I. Vurgaftman, S.J. Sweeney. J. Phys. D: Appl. Phys., **54**, 055105 (2021).
[42] V.Ya. Aleshkin, V.V. Rumyantsev, K.E. Kudryavtsev, A.A. Dubinov, V.V. Utochkin, M.A. Fadeev, G. Alymov, N.N. Mikhailov, S.A. Dvoretsky, F. Teppe, V.I. Gavrilenko, S.V. Morozov. J. Appl. Phys., **129**, 133106 (2021).
[43] K.E. Kudryavtsev, A.A. Yantser, M.A. Fadeev, V.V. Rumyantsev, A.A. Dubinov, V.Ya. Aleshkin, N.N. Mikhailov, S.A. Dvoretsky, V.I. Gavrilenko, S.V. Morozov. Appl. Phys. Lett., **123**, 18 (2013).

Translated by A.Akhtyamov